Western Blot Analyses

Western blot analysis was performed as described.[46,47] Briefly, isolated glomeruli were homogenized in cold RIPA buffer (50 mM Tris-HCl, 150 mM NaCl, 4 mM EDTA, 1% Nonidet P-40, 0.1% sodium deoxycholate, 10 mM $Na_4P_2O_7$, 10 mM NaF, 10 μg/ml aprotinin, 2 mM dithiothreitol, 2 mM sodium orthovanadate, and 1 mM PMSF). For cultured cells, cells were lysed with RIPA buffer for ERK detection, or were processed with the AllPrep DNA/RNA/protein Mini kit and then lysed with lysis buffer containing 100 mM Tris-HCl, 3% SDS, 10 mM $NaHPO_4$, 1% Nonidet P-40, 20 mM EDTA, 10 μg/ml aprotinin, 2 mM dithiothreitol, 2 mM sodium orthovanadate, and 1 mM PMSF for p38 MAPK detection. The homogenates were centrifuged at 15,000 rpm for 15 minutes at 4°C, and the supernatants were treated with NuPAGE sample buffer (Invitrogen, Carlsbad, CA). Western blot analysis was performed as described with some modifications using NuPAGE Bis-Tris gels (Invitrogen).[47] Filters on isolated cell extracts were incubated with rabbit anti-phospho-p44/p42 MAPK antibody or anti-phospho-p38 MAPK antibody for 1 hour, and immunoblots were developed using horseradish peroxidase-linked donkey anti-rabbit antibodies (Amersham, Arlington Heights, IL) and a chemiluminescence kit (Amersham).

Statistical Analyses

Data are expressed as the mean ± SEM. Statistical analysis was performed using one-way ANOVA. $P<0.05$ was considered statistically significant.

ACKNOWLEDGMENTS

We gratefully acknowledge Mr. M. Fujimoto and Mr. Y. Sakashita and other laboratory members for technical assistance and Ms. A. Yamamoto for secretarial assistance.

This work was supported in part by research grants from the Japanese Ministry of Education, Culture, Sports, Science, and Technology; the Japanese Ministry of Health, Labour, and Welfare; and the Salt Science Research Foundation.

DISCLOSURES

None.

REFERENCES

1. Nishimura M, Uzu T, Fujii T, Kuroda S, Nakamura S, Inenaga T, Kimura G: Cardiovascular complications in patients with primary aldosteronism. *Am J Kidney Dis* 33: 261–266, 1999
2. Schrier RW, Masoumi A, Elhassan E: Aldosterone: Role in edematous disorders, hypertension, chronic renal failure, and metabolic syndrome. *Clin J Am Soc Nephrol* 5: 1132–1140, 2010
3. Ribstein J, Du Cailar G, Fesler P, Mimran A: Relative glomerular hyperfiltration in primary aldosteronism. *J Am Soc Nephrol* 16: 1320–1325, 2005
4. Greene EL, Kren S, Hostetter TH: Role of aldosterone in the remnant kidney model in the rat. *J Clin Invest* 98: 1063–1068, 1996
5. Klar J, Vitzthum H, Kurtz A: Aldosterone enhances renin gene expression in juxtaglomerular cells. *Am J Physiol Renal Physiol* 286: F349–F355, 2004
6. Harada E, Yoshimura M, Yasue H, Nakagawa O, Nakagawa M, Harada M, Mizuno Y, Nakayama M, Shimasaki Y, Ito T, Nakamura S, Kuwahara K, Saito Y, Nakao K, Ogawa H: Aldosterone induces angiotensin-converting-enzyme gene expression in cultured neonatal rat cardiocytes. *Circulation* 104: 137–139, 2001
7. Briet M, Schiffrin EL: Aldosterone: Effects on the kidney and cardiovascular system. *Nat Rev Nephrol* 6: 261–273, 2010
8. Nishiyama A, Yao L, Nagai Y, Miyata K, Yoshizumi M, Kagami S, Kondo S, Kiyomoto H, Shokoji T, Kimura S, Kohno M, Abe Y: Possible contributions of reactive oxygen species and mitogen-activated protein kinase to renal injury in aldosterone/salt-induced hypertensive rats. *Hypertension* 43: 841–848, 2004
9. Terada Y, Kobayashi T, Kuwana H, Tanaka H, Inoshita S, Kuwahara M, Sasaki S: Aldosterone stimulates proliferation of mesangial cells by activating mitogen-activated protein kinase 1/2, cyclin D1, and cyclin A. *J Am Soc Nephrol* 16: 2296–2305, 2005
10. Mundel P, Reiser J: Proteinuria: An enzymatic disease of the podocyte? *Kidney Int* 77: 571–580, 2010
11. Nagase M, Shibata S, Yoshida S, Nagase T, Gotoda T, Fujita T: Podocyte injury underlies the glomerulopathy of Dahl salt-hypertensive rats and is reversed by aldosterone blocker. *Hypertension* 47: 1084–1093, 2006
12. Shibata S, Nagase M, Yoshida S, Kawachi H, Fujita T: Podocyte as the target for aldosterone: Roles of oxidative stress and Sgk1. *Hypertension* 49: 355–364, 2007
13. Shibata S, Nagase M, Yoshida S, Kawarazaki W, Kurihara H, Tanaka H, Miyoshi J, Takai Y, Fujita T: Modification of mineralocorticoid receptor function by Rac1 GTPase: Implication in proteinuric kidney disease. *Nat Med* 14: 1370–1376, 2008
14. Nakao K, Ogawa Y, Suga S, Imura H: Molecular biology and biochemistry of the natriuretic peptide system. I: Natriuretic peptides. *J Hypertens* 10: 907–912, 1992
15. Sugawara A, Nakao K, Morii N, Yamada T, Itoh H, Shiono S, Saito Y, Mukoyama M, Arai H, Nishimura K, Obata K, Yasue H, Ban T, Imura H: Synthesis of atrial natriuretic polypeptide in human failing hearts. Evidence for altered processing of atrial natriuretic polypeptide precursor and augmented synthesis of β-human ANP. *J Clin Invest* 81: 1962–1970, 1988
16. Mukoyama M, Nakao K, Hosoda K, Suga S, Saito Y, Ogawa Y, Shirakami G, Jougasaki M, Obata K, Yasue H, Kambayashi Y, Inouye K, Imura H: Brain natriuretic peptide as a novel cardiac hormone in humans. Evidence for an exquisite dual natriuretic peptide system, atrial natriuretic peptide and brain natriuretic peptide. *J Clin Invest* 87: 1402–1412, 1991
17. Potter LR, Abbey-Hosch S, Dickey DM: Natriuretic peptides, their receptors, and cyclic guanosine monophosphate-dependent signaling functions. *Endocr Rev* 27: 47–72, 2006
18. Ritter D, Dean AD, Gluck SL, Greenwald JE: Natriuretic peptide receptors A and B have different cellular distributions in rat kidney. *Kidney Int* 48: 5758–5766, 1995
19. Lopez MJ, Wong SK, Kishimoto I, Dubois S, Mach V, Friesen J, Garbers DL, Beuve A: Salt-resistant hypertension in mice lacking the guanylyl cyclase-A receptor for atrial natriuretic peptide. *Nature* 378: 65–68, 1995
20. Kishimoto I, Rossi K, Garbers DL: A genetic model provides evidence that the receptor for atrial natriuretic peptide (guanylyl cyclase-A) inhibits cardiac ventricular myocyte hypertrophy. *Proc Natl Acad Sci USA* 98: 2703–2706, 2001
21. Kishimoto I, Dubois SK, Garbers DL: The heart communicates with the kidney exclusively through the guanylyl cyclase-A receptor: Acute handling of sodium and water in response to volume expansion. *Proc Natl Acad Sci USA* 93: 6215–6219, 1996

22. Conger JD, Falk SA, Hammond WS: Atrial natriuretic peptide and dopamine in established acute renal failure in the rat. *Kidney Int* 40: 21–28, 1991
23. Nigwekar SU, Navaneethan SD, Parikh CR, Hix JK: Atrial natriuretic peptide for management of acute kidney injury: A systematic review and meta-analysis. *Clin J Am Soc Nephrol* 4: 261–272, 2009
24. Kasahara M, Mukoyama M, Sugawara A, Makino H, Suganami T, Ogawa Y, Nakagawa M, Yahata K, Goto M, Ishibashi R, Tamura N, Tanaka I, Nakao K: Ameliorated glomerular injury in mice overexpressing brain natriuretic peptide with renal ablation. *J Am Soc Nephrol* 11: 1691–1701, 2000
25. Suganami T, Mukoyama M, Sugawara A, Mori K, Nagae T, Kasahara M, Yahata K, Makino H, Fujinaga Y, Ogawa Y, Tanaka I, Nakao K: Overexpression of brain natriuretic peptide in mice ameliorates immune-mediated renal injury. *J Am Soc Nephrol* 12: 2652–2663, 2001
26. Makino H, Mukoyama M, Mori K, Suganami T, Kasahara M, Yahata K, Nagae T, Yokoi H, Sawai K, Ogawa Y, Suga S, Yoshimasa Y, Sugawara A, Tanaka I, Nakao K: Transgenic overexpression of brain natriuretic peptide prevents the progression of diabetic nephropathy in mice. *Diabetologia* 49: 2514–2524, 2006
27. Opgenorth TJ, Burnett JC Jr, Granger JP, Scriven TA: Effects of atrial natriuretic peptide on renin secretion in nonfiltering kidney. *Am J Physiol* 250: F798–F801, 1986
28. Ito T, Yoshimura M, Nakamura S, Nakayama M, Shimasaki Y, Harada E, Mizuno Y, Yamamuro M, Harada M, Saito Y, Nakao K, Kurihara H, Yasue H, Ogawa H: Inhibitory effect of natriuretic peptides on aldosterone synthase gene expression in cultured neonatal rat cardiocytes. *Circulation* 107: 807–810, 2003
29. Bedard K, Krause KH: The NOX family of ROS-generating NADPH oxidases: Physiology and pathophysiology. *Physiol Rev* 87: 245–313, 2007
30. Vellaichamy E, Zhao D, Somanna N, Pandey KN: Genetic disruption of guanylyl cyclase/natriuretic peptide receptor-A upregulates ACE and AT1 receptor gene expression and signaling: Role in cardiac hypertrophy. *Physiol Genomics* 31: 193–202, 2007
31. Hoffmann S, Podlich D, Hähnel B, Kriz W, Gretz N: Angiotensin II type 1 receptor overexpression in podocytes induces glomerulosclerosis in transgenic rats. *J Am Soc Nephrol* 15: 1475–1487, 2004
32. Crowley SD, Vasievich MP, Ruiz P, Gould SK, Parsons KK, Pazmino AK, Facemire C, Chen BJ, Kim HS, Tran TT, Pisetsky DS, Barisoni L, Prieto-Carrasquero MC, Jeansson M, Foster MH, Coffman TM: Glomerular type 1 angiotensin receptors augment kidney injury and inflammation in murine autoimmune nephritis. *J Clin Invest* 119: 943–953, 2009
33. Golos M, Lewko B, Bryl E, Witkowski JM, Dubaniewicz A, Olszewska A, Latawiec E, Angielski S, Stepinski J: Effect of angiotensin II on ANP-dependent guanylyl cyclase activity in cultured mouse and rat podocytes. *Kidney Blood Press Res* 25: 296–302, 2002
34. Baldini PM, De Vito P, D'aquilio F, Vismara D, Zalfa F, Bagni C, Fiaccavento R, Di Nardo P: Role of atrial natriuretic peptide in the suppression of lysophosphatydic acid-induced rat aortic smooth muscle (RASM) cell growth. *Mol Cell Biochem* 272: 19–28, 2005
35. Bilzer M, Jaeschke H, Vollmar AM, Paumgartner G, Gerbes AL: Prevention of Kupffer cell-induced oxidant injury in rat liver by atrial natriuretic peptide. *Am J Physiol* 276: G1137–G1144, 1999
36. Modlinger PS, Wilcox CS, Aslam S: Nitric oxide, oxidative stress, and progression of chronic renal failure. *Semin Nephrol* 24: 354–365, 2004
37. Pergola PE, Raskin P, Toto RD, Meyer CJ, Huff JW, Grossman EB, Krauth M, Ruiz S, Audhya P, Christ-Schmidt H, Wittes J, Warnock DG; BEAM Study Investigators: Bardoxolone methyl and kidney function in CKD with type 2 diabetes. *N Engl J Med* 365: 327–336, 2011
38. Jiang T, Huang Z, Lin Y, Zhang Z, Fang D, Zhang DD: The protective role of Nrf2 in streptozotocin-induced diabetic nephropathy. *Diabetes* 59: 850–860, 2010
39. Thalhamer T, McGrath MA, Harnett MM: MAPKs and their relevance to arthritis and inflammation. *Rheumatology (Oxford)* 47: 409–414, 2008
40. Kim EK, Choi EJ: Pathological roles of MAPK signaling pathways in human diseases. *Biochim Biophys Acta* 1802: 396–405, 2010
41. Koshikawa M, Mukoyama M, Mori K, Suganami T, Sawai K, Yoshioka T, Nagae T, Yokoi H, Kawachi H, Shimizu F, Sugawara A, Nakao K: Role of p38 mitogen-activated protein kinase activation in podocyte injury and proteinuria in experimental nephrotic syndrome. *J Am Soc Nephrol* 16: 2690–2701, 2005
42. Yaoita E, Yao J, Yoshida Y, Morioka T, Nameta M, Takata T, Kamiie J, Fujinaka H, Oite T, Yamamoto T: Up-regulation of connexin43 in glomerular podocytes in response to injury. *Am J Pathol* 161: 1597–1606, 2002
43. Stephens RS, Rentsendorj O, Servinsky LE, Moldobaeva A, Damico R, Pearse DB: cGMP increases antioxidant function and attenuates oxidant cell death in mouse lung microvascular endothelial cells by a protein kinase G-dependent mechanism. *Am J Physiol Lung Cell Mol Physiol* 299: L323–L333, 2010
44. Takahashi N, Saito Y, Kuwahara K, Harada M, Kishimoto I, Ogawa Y, Kawakami R, Nakagawa Y, Nakanishi M, Nakao K: Angiotensin II-induced ventricular hypertrophy and extracellular signal-regulated kinase activation are suppressed in mice overexpressing brain natriuretic peptide in circulation. *Hypertens Res* 26: 847–853, 2003
45. Schrier RW, Abraham WT: Hormones and hemodynamics in heart failure. *N Engl J Med* 341: 577–585, 1999
46. Yokoi H, Mukoyama M, Mori K, Kasahara M, Suganami T, Sawai K, Yoshioka T, Saito Y, Ogawa Y, Kuwabara T, Sugawara A, Nakao K: Overexpression of connective tissue growth factor in podocytes worsens diabetic nephropathy in mice. *Kidney Int* 73: 446–455, 2008
47. Yokoi H, Mukoyama M, Nagae T, Mori K, Suganami T, Sawai K, Yoshioka T, Koshikawa M, Nishida T, Takigawa M, Sugawara A, Nakao K: Reduction in connective tissue growth factor by antisense treatment ameliorates renal tubulointerstitial fibrosis. *J Am Soc Nephrol* 15: 1430–1440, 2004

This article contains supplemental material online at http://jasn.asnjournals.org/lookup/suppl/doi:10.1681/ASN.2011100985/-/DCSupplemental.

The EMBO Journal (2012) 31, 4428–4440 | © 2012 European Molecular Biology Organization | All Rights Reserved 0261-4189/12
www.embojournal.org

THE EMBO JOURNAL

Reciprocal expression of MRTF-A and myocardin is crucial for pathological vascular remodelling in mice

Takeya Minami[1], Koichiro Kuwahara[1,*], Yasuaki Nakagawa[1], Minoru Takaoka[2], Hideyuki Kinoshita[1], Kazuhiro Nakao[1], Yoshihiro Kuwabara[1], Yuko Yamada[1], Chinatsu Yamada[1], Junko Shibata[1], Satoru Usami[1], Shinji Yasuno[3], Toshio Nishikimi[1], Kenji Ueshima[3], Masataka Sata[4], Hiroyasu Nakano[5], Takahiro Seno[6], Yutaka Kawahito[6], Kenji Sobue[7], Akinori Kimura[8], Ryozo Nagai[2] and Kazuwa Nakao[1]

[1]Department of Medicine and Clinical Science, Kyoto University Graduate School of Medicine, Kyoto, Japan, [2]Department of Cardiovascular Medicine, Graduate School of Medicine, The University of Tokyo, Tokyo, Japan, [3]EBM Research Center, Kyoto University Graduate School of Medicine, Kyoto, Japan, [4]Department of Cardiovascular Medicine, Institute of Health Biosciences, The University of Tokushima Graduate School, Tokushima, Japan, [5]Laboratory of Molecular and Biochemical Research, Department of Immunology, Biomedical Research Center, Juntendo University Graduate School of Medicine, Tokyo, Japan, [6]Department of Inflammation and Immunology, Graduate School of Medical Science, Kyoto Prefectural University of Medicine, Kyoto, Japan, [7]Department of Neuroscience, Institute for Biomedical Sciences, Iwate Medical University, Iwate, Japan and [8]Department of Molecular Pathogenesis, Medical Research Institute, Tokyo Medical and Dental University, Tokyo, Japan

Myocardin-related transcription factor (MRTF)-A is a Rho signalling-responsive co-activator of serum response factor (SRF). Here, we show that induction of MRTF-A expression is key to pathological vascular remodelling. MRTF-A expression was significantly higher in the wire-injured femoral arteries of wild-type mice and in the atherosclerotic aortic tissues of ApoE$^{-/-}$ mice than in healthy control tissues, whereas myocardin expression was significantly lower. Both neointima formation in wire-injured femoral arteries in MRTF-A knockout (*Mkl1*$^{-/-}$) mice and atherosclerotic lesions in *Mkl1*$^{-/-}$; *ApoE*$^{-/-}$ mice were significantly attenuated. Expression of vinculin, matrix metallopeptidase 9 (MMP-9) and integrin β1, three SRF targets and key regulators of cell migration, in injured arteries was significantly weaker in *Mkl1*$^{-/-}$ mice than in wild-type mice. In cultured vascular smooth muscle cells (VSMCs), knocking down MRTF-A reduced expression of these genes and significantly impaired cell migration. Underlying the increased MRTF-A expression in dedifferentiated VSMCs was the downregulation of microRNA-1. Moreover, the MRTF-A inhibitor CCG1423 significantly reduced neointima formation following wire injury in mice. MRTF-A could thus be a novel therapeutic target for the treatment of vascular diseases.

The EMBO Journal (2012) **31,** 4428–4440. doi:10.1038/emboj.2012.296; Published online 26 October 2012
Subject Categories: molecular biology of disease
Keywords: atherosclerosis; muscle, smooth; remodelling; signal transduction

Introduction

It is now recognized that modulation of vascular smooth muscle cell (VSMC) phenotypes plays a key role in the progression of several prominent cardiovascular disease states, including atherosclerosis, hypertension and restenosis (Schwartz *et al*, 1995; Owens *et al*, 2004). Pathological stress induces a switch from a differentiated VSMC phenotype, characterized by strong expression of contractile proteins and little capacity for migration or proliferation, to a proliferative dedifferentiated phenotype, characterized by relatively weak expression of contractile proteins and an increased capacity for migration and proliferation (Watanabe *et al*, 1999; Owens *et al*, 2004; Nishimura *et al*, 2006). VSMC proliferation and migration contribute to vascular remodelling and obstructive vasculopathies such as atherosclerosis and restenosis following percutaneous coronary intervention (Schwartz *et al*, 1995; Bentzon *et al*, 2006). Cytokines and growth factors locally secreted from cells within the vessel and infiltrating inflammatory cells induce migratory and proliferative responses in VSMCs during vascular remodelling (Owens *et al*, 2004), but the intracellular signalling pathways and the transcriptional regulators of phenotypic modulation of VSMCs are incompletely understood.

Myocardin, myocardin-related transcription factor (MRTF)-A (Mkl1, Bsac or Mal) and MRTF-B (Mkl2) are transcriptional cofactors that associate with serum response factor (SRF), an MADS box transcription factor and critical modulator of cardiovascular differentiation and growth, promoting transcription of a subset of genes involved in cytoskeletal organization and muscle differentiation (Wang *et al*, 2001, 2002; Miano, 2003; Olson and Nordheim, 2010). Myocardin, which is highly restricted to smooth and cardiac muscle cell lineages, is located constitutively in the nucleus and strongly activates transcription of SRF-regulated genes, thereby playing an important role in the differentiation and maintenance of cardiac and smooth muscle cell lineage. By contrast, MRTF-A and -B are expressed more ubiquitously and are found in both the cytoplasm and nucleus. In serum-starved fibroblasts, MRTF-A and -B are localized mainly in the cytoplasm and are translocated into the nucleus in response to stimulation with serum or other

*Corresponding author. Department of Medicine and Clinical Science, Kyoto University Graduate School of Medicine, 54 Shogoin Kawaharacho, Sakyo-ku, Kyoto 606-8507, Japan. Tel.: +81 75 751 4287; Fax: +81 75 771 9452; E-mail: kuwa@kuhp.kyoto-u.ac.jp

Received: 13 May 2012; accepted: 2 October 2012; published online: 26 October 2012

stimuli that promote Rho family GTPase activation and subsequent actin polymerization (Kuwahara *et al*, 2005; Nakamura *et al*, 2010; Olson and Nordheim, 2010). Thus, MRTF-A and -B transduce Rho family GTPase-actin signalling from the cytoplasm to SRF in the nucleus (Miralles *et al*, 2003).

Myocardin knockout leads to death *in utero* due to defects in vascular development (Li *et al*, 2003). In addition, myocardin mRNA levels have been shown to be downregulated in dedifferentiated VSMCs during vascular diseases (Liu *et al*, 2005; Chen *et al*, 2011). In contrast to myocardin, the roles played by MRTF-A in VSMC differentiation and phenotypic modulation remain unclear, though a recent human genetic analysis detected an association between coronary artery disease (CAD) and a single-nucleotide polymorphism (SNP) in the promoter region of the MRTF-A gene that enhances the gene expression (Hinohara *et al*, 2009). Li *et al* (2006) reported that MRTF-A knockout mice were born in anticipated Mendelian ratios, whereas Sun *et al* (2006) reported that MRTF-A knockout mice were born at less than the anticipated Mendelian ratio, which they attributed to fetal loss due to heart failure. In both groups, however, live born MRTF-A knockout pups showed no obvious gross abnormality or cardiovascular defect under normal conditions, except for a defect in maternal lactation due to impaired phenotypic modulation of mammary gland myoepithelial cells (Li *et al*, 2006; Sun *et al*, 2006).

In the present study, we investigated the potential roles of MRTF-A in the pathological processes underlying vascular proliferative diseases. We found that induction of MRTF-A expression is key to pathological remodelling underlying vascular disorders, as it sustains the SRF activity necessary for dedifferentiated VSMCs to acquire the capacity to migrate in response to extracellular stimuli. Our findings suggest that the reciprocal expression of MRTF-A and myocardin is mediated, at least in part, by microRNA (miR)-1 and contributes to the phenotypic modulation of VSMCs during vascular remodelling. These results point to MRTF-A as a potentially useful therapeutic target for the treatment of vascular diseases.

Results

Increased expression of MRTF-A in femoral arteries after wire injury

To explore the potential role played by MRTF-A during pathological vascular remodelling, we initially compared the expression of myocardin, MRTF-A and MRTF-B mRNA between femoral arteries subjected to wire injury or to a sham operation. As seen previously (Liu *et al*, 2005; Chen *et al*, 2011), levels of myocardin mRNA were significantly downregulated in femoral arteries 2 weeks after wire injury, while levels of MRTF-B mRNA were not significantly affected (Figure 1A). By contrast, expression of MRTF-A mRNA was significantly increased in injured arteries, as compared to sham-operated arteries (Figure 1A). Western blot analysis using specific antibodies for myocardin, MRTF-A and MRTF-B, respectively, clearly showed that the level of myocardin protein was reduced in injured arteries, whereas MRTF-A protein was significantly increased (Figure 1B and C; Supplementary Figure S1A). Immunohistochemical analysis showed that cells positively stained for MRTF-A were located mainly in the neointima of injured arteries (Figure 1D; Supplementary Figure S1B). Moreover, in serial sections stained for α-smooth muscle actin (αSMA) and smooth muscle myosin heavy chain (SM-MHC), most of the cells that positively stained for MRTF-A also positively stained for both αSMA and SM-MHC (Figure 1D). Time-course analysis of MRTF-A and myocardin expression revealed that MRTF-A mRNA levels were significantly increased by 2 weeks after injury, when dedifferentiated neointimal VSMCs expressing a relatively low level of αSMA were increasing (Shoji *et al*, 2004; Daniel *et al*, 2010). By 50 days after injury, when a more differentiated population of VSMCs is restored (Daniel *et al*, 2010), MRTF-A mRNA had declined to levels comparable to those seen on day 0 (Supplementary Figure S1C). By contrast, myocardin mRNA levels declined continuously for 2 weeks after injury, but had recovered by 50 days after injury (Supplementary Figure S1D). These results suggest that MRTF-A expression is upregulated in activated, dedifferentiated VSMCs during vascular remodelling, while myocardin expression is downregulated in these cells.

Attenuated vascular remodelling after wire injury in MRTF-A knockout mice

To further evaluate the function of MRTF-A during vascular remodelling, next we performed wire injury in the femoral arteries of MRTF-A knockout ($Mkl1^{-/-}$) mice. As previously reported, the $Mkl1^{-/-}$ mice were viable, fertile and showed no significant gross abnormalities or cardiovascular defects under normal conditions (Li *et al*, 2006). There was no difference in blood pressure or heart rate between wild-type and $Mkl1^{-/-}$ mice (Figure 2A), and the thickness of the medial wall in the uninjured sham-operated femoral arteries was comparable between wild-type and $Mkl1^{-/-}$ mice (Table I). Femoral arterial expression of myocardin mRNA was significantly weaker in $Mkl1^{-/-}$ mice 2 weeks after wire injury than in sham-operated arteries, just as was observed with wild-type mice (Figure 2B). On the other hand, neointima-to-medial ratios determined 4 weeks after wire injury were significantly smaller in $Mkl1^{-/-}$ mice than in wild-type mice, whereas there was no difference in medial thickness in the injured arteries between wild-type and $Mkl1^{-/-}$ mice (Figure 2C and D; Table I).

Four weeks after wire injury, the neointimal area comprised cells positively stained for αSMA was markedly smaller in $Mkl1^{-/-}$ mice than in wild-type mice (Figure 2D). Immunohistochemical analysis in serial sections stained for SM-MHC showed overlap with αSMA-positive cells (Figure 2D), suggesting that a reduction in the numbers of dedifferentiated VSMCs within the neointima is largely responsible for the reduction in the neointima-to-medial ratios seen in $Mkl1^{-/-}$ mice. Indeed, the numbers of Ki-67-positive proliferating cells within the injured vessels were also significantly lower in $Mkl1^{-/-}$ mice than in wild-type mice (Figure 2E and F). By contrast, the numbers of TUNEL-positive or cleaved caspase-3-positive apoptotic cells within the injured arteries did not differ between wild-type and $Mkl1^{-/-}$ mice (Supplementary Figure S2A through D). Similarly, the % fibrotic area in the media and intima and expression of the genes encoding collagen type 1 alpha1 and collagen type3 alpha1 within the injured arteries also did not significantly differ between wild-type and $Mkl1^{-/-}$ mice

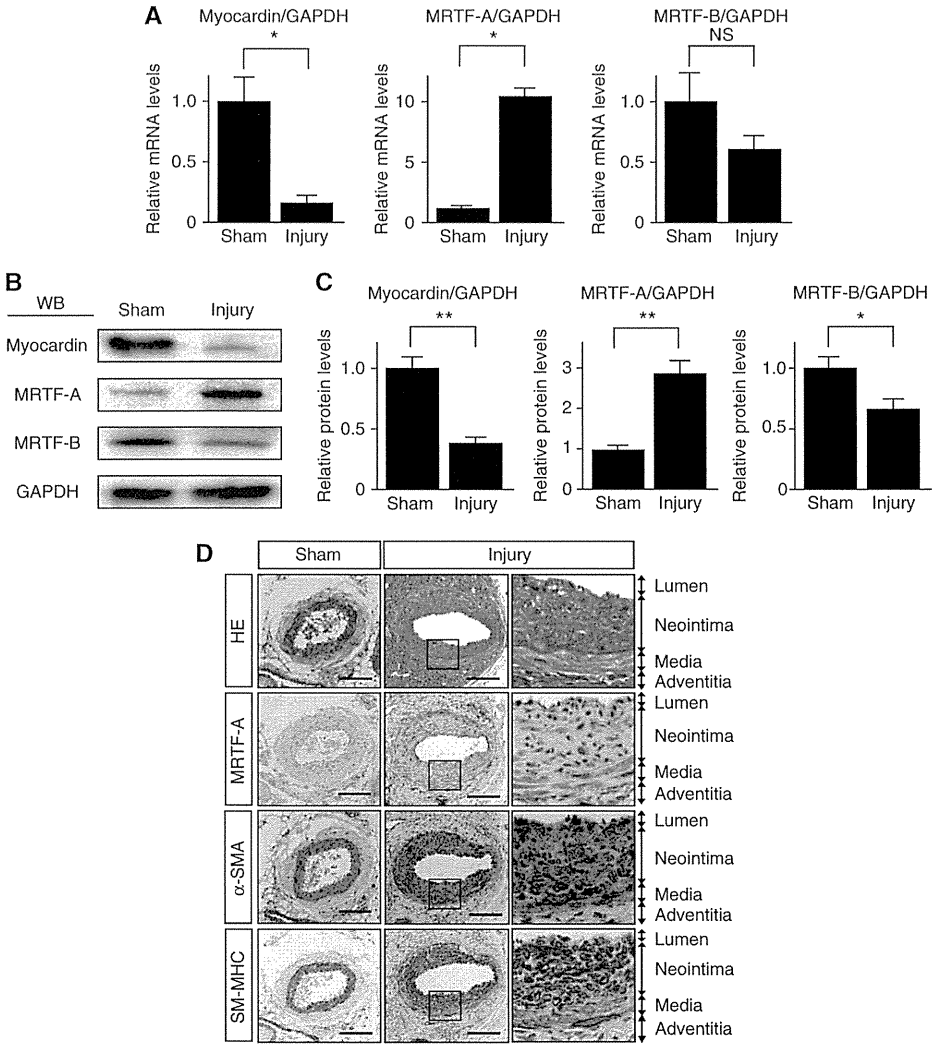

Figure 1 Increased expression of MRTF-A in femoral arteries after wire injury in mice. (**A**) Real-time RT–PCR analysis showing relative levels of myocardin, MRTF-A and MRTF-B mRNAs (normalized to GAPDH mRNA) in femoral arteries 2 weeks after wire injury (injury) ($n=6$ each). The relative mRNA level in sham-operated arteries (sham) was assigned a value of 1.0. (**B**) Representative western blots showing myocardin, MRTF-A and MRTF-B in wire-injured and sham-operated femoral arteries (2 weeks after injury). (**C**) The relative protein levels (normalized to GAPDH) of myocardin, MRTF-A and MRTF-B in wire-injured and sham-operated femoral arteries ($n=4$ each). The relative protein level in the sham-operated arteries was assigned a value of 1.0. (**D**) Immunohistochemical analysis of MRTF-A expression in sham-operated and wire-injured femoral arteries. Tissues are labelled with anti-BSAC (MRTF-A), anti-α-smooth muscle actin (αSMA) or anti-smooth muscle myosin heavy chain (SM-MHC) antibodies; bar indicates 100 μm. Three different experiments gave identical results. All graphs are shown as means ± s.e.m. $^*P<0.05$. $^{**}P<0.001$. NS, not significant. Figure source data can be found with the Supplementary data.

(Supplementary Figure S2E through G). In addition, because multiple cell types other than dedifferentiated VSMCs can contribute to neointima formation and to the vascular remodelling process, we also stained the tissue for endothelial cell (CD31) and macrophage (Mac3) markers. The relative numbers of CD31-positive and Mac3-positive cells in the injured arteries did not differ between wild-type and *Mkl1*$^{-/-}$ mice (Figure 2G through I), which indicates that a reduction in the number of αSMA-positive dedifferentiated VSMCs contributes to the attenuation of vascular remodelling in wire-injured *Mkl1*$^{-/-}$ mice. We also examined neointima formation following carotid artery ligation in *Mkl1*$^{-/-}$ mice, and found that neointima formation 4 weeks after carotid ligation was significantly diminished in *Mkl1*$^{-/-}$ mice, as compared to control *Mkl*$^{+/-}$ mice (Supplementary Figure S2H and I; Supplementary Table S1).

Loss of MRTF-A attenuates atherosclerotic lesions in APOE$^{-/-}$ *mice*

We next sought to analyse MRTF-A expression in a model of a different type of vascular disorder. *ApoE*$^{-/-}$ mice are prone to atherosclerotic lesions, to which both dedifferentiated VSMCs and infiltrating inflammatory cells contribute (Glass and Witztum, 2001; Bentzon *et al*, 2006). MRTF-A gene expression was significantly upregulated in aortic tissues containing atherosclerotic lesions in *ApoE*$^{-/-}$ mice fed a high cholesterol diet for 8 weeks (from 8 to 16 weeks of age), as compared to normal wild-type aortic tissues in

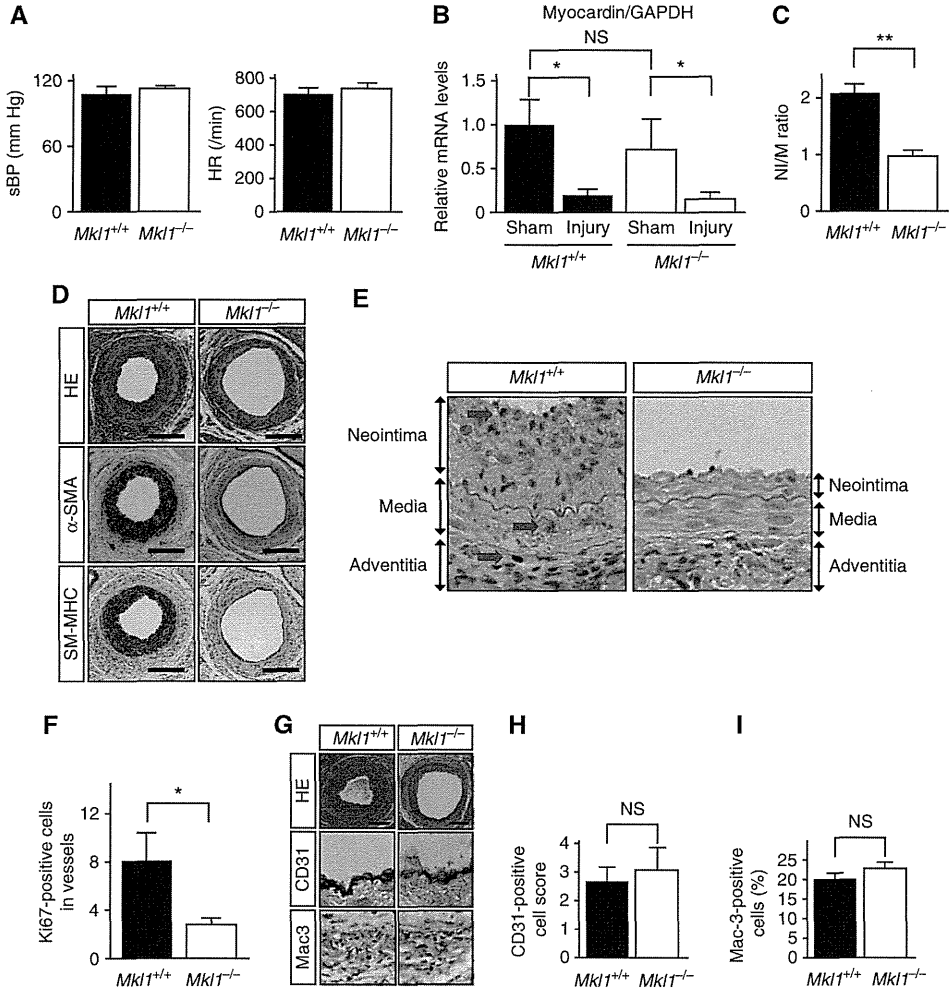

Figure 2 Attenuated vascular remodelling in response to wire injury in *Mkl1*$^{-/-}$ mice. (**A**) Systolic blood pressure (sBP) and heart rate (HR) in control *Mkl1*$^{+/+}$ and *Mkl1*$^{-/-}$ mice ($n=5$ each). (**B**) The relative levels of myocardin mRNA in wire-injured and sham-operated femoral arteries in *Mkl1*$^{+/+}$ and *Mkl1*$^{-/-}$ mice ($n=5$ each). (**C**) The neointima (NI)-to-media (M) ratio in arteries 4 weeks after wire injury in *Mkl1*$^{+/+}$ and *Mkl1*$^{-/-}$ mice ($n=20$ each). (**D**) Representative images of neointima in arteries 4 weeks after wire injury in *Mkl1*$^{+/+}$ and *Mkl1*$^{-/-}$ mice. HE: haematoxylin-eosin staining. α-SMA: staining with anti-α-SMA antibody. SM-MHC: staining with anti-SM-MHC antibody. (**E**) Representative images of neointima 4 weeks after femoral artery injury stained with anti-Ki-67 antigen in *Mkl1*$^{+/-}$ and *Mkl1*$^{-/-}$ mice. Red arrows indicate Ki-67-positive cells. (**F**) Numbers of Ki-67-positive cells in injured vessels of *Mkl1*$^{+/+}$ and *Mkl1*$^{-/-}$ mice 4 weeks after wire injury are shown ($n=3$ in each group). (**G**) Representative images of neointima stained with anti-CD31 (CD31) or anti-Mac3 (Mac3) antibody in arteries from *Mkl1*$^{+/+}$ and *Mkl1*$^{-/-}$ mice 4 weeks after wire injury. (**H, I**) The semi-quantitative CD31-positive scores ($n=5$ in each group) (**H**) and the relative numbers of Mac3-positive cells (% positive cells/total cells in neointima and media; $n=4$ in each group) (**I**) in *Mkl1*$^{+/+}$ and *Mkl1*$^{-/-}$ mice 4 weeks after wire injury are shown. All graphs are shown as means ± s.e.m. *$P<0.05$. **$P<0.001$. NS, not significant.

Table I Luminal and neointimal area of femoral arteries 4 weeks after vascular injury

	n	Lumen ($\times 10^3/\mu m^2$)	Intima ($\times 10^3/\mu m^2$)	Media ($\times 10^3/\mu m^2$)	IEL ($\times 10^3/\mu m^2$)	EEL ($\times 10^3/\mu m^2$)	Intima/Media ratio
Mkl1$^{+/+}$ sham	4	11.9 ± 2.7	0	19.0 ± 1.2	11.9 ± 2.7	30.9 ± 3.3	0
Mkl1$^{-/-}$ sham	4	10.4 ± 2.8	0	20.2 ± 2.5	10.4 ± 2.8	30.6 ± 2.8	0
Mkl1$^{+/+}$ injury	20	24.9 ± 3.5	39.7 ± 5.0	18.8 ± 1.1	64.8 ± 4.6	84.0 ± 5.4	2.09 ± 0.17
Mkl1$^{-/-}$ injury	20	29.6 ± 3.9	22.0 ± 2.3*	22.7 ± 1.2	52.3 ± 4.6	75.3 ± 5.3	0.96 ± 0.10*

The ratio of intima to media was calculated as the intimal area/medial area. Values are means ± s.e.m. IEL, internal elastic lamina; EEL, external elastic lamina. *$P<0.01$ versus *Mkl1*$^{+/+}$ injured arteries.

age-matched mice (Figure 3A). By contrast, myocardin gene expression was significantly decreased in atherosclerotic aortas, compared to normal aortas (Figure 3A). Consistent with that finding, cells positively stained for MRTF-A were observed within atherosclerotic lesions in the proximal aorta of *ApoE*$^{-/-}$ mice (Figure 3B).

To evaluate directly the contribution of MRTF-A to the development of atherosclerotic lesions in *ApoE*$^{-/-}$ mice, we crossed *Mkl1*$^{-/-}$ and *Apo E*$^{-/-}$ mice. Although the blood pressures, heart rates, cholesterol profiles and myocardin gene expression in aortic tissues did not differ between *Mkl1*$^{+/+}$;*ApoE*$^{-/-}$ and *Mkl1*$^{-/-}$;*ApoE*$^{-/-}$ mice

(Supplementary Figure S3A; Figure 3C), en-face analysis of the global progression of atherosclerotic lesions throughout the aorta revealed that the aortas of $Mkl1^{-/-}$;$ApoE^{-/-}$ mice contained smaller atherosclerotic lesions than those of $Mkl1^{+/+}$;$ApoE^{-/-}$ mice (Figure 3D). Furthermore, cross-sectional analysis of the proximal aorta revealed the average lesion area at the aortic root of $Mkl1^{-/-}$;$ApoE^{-/-}$ mice (2.5%) to be significantly smaller than at the aortic root of $Mkl1^{+/+}$; $ApoE^{-/-}$ mice (11.8%, $P<0.05$ versus $Mkl1^{-/-}$;$ApoE^{-/-}$) (Figure 3E and F). The relative accumulation of macrophages within atherosclerotic lesions at the aortic root, which was estimated based on the size of the

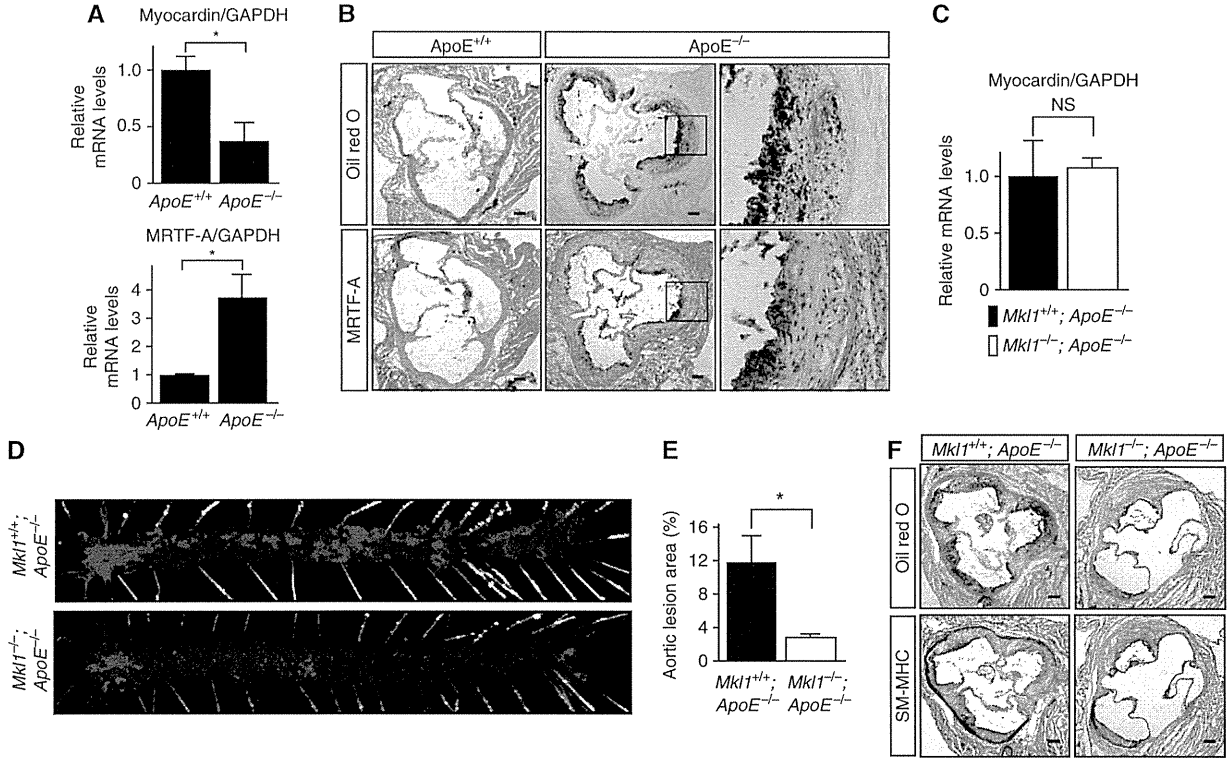

Figure 3 Atherosclerotic lesions in $Mkl1^{-/-}$;$ApoE^{-/-}$ mice are attenuated, as compared to those in $Mkl1^{+/+}$;$ApoE^{-/-}$ mice. (**A**) Real-time RT–PCR analysis showing the relative levels of MRTF-A and myocardin mRNAs (normalized to GAPDH mRNA) in atherosclerotic aortas from $ApoE^{-/-}$ mice fed a high-cholesterol diet and normal aortas from $ApoE^{+/+}$ mice at 16 weeks of age ($n=4$ each). *$P<0.05$. (**B**) Representative images showing MRTF-A expression within an atherosclerotic lesion in the proximal aorta of $ApoE^{-/-}$ mice. The tissues from $Apo^{+/+}$ and $ApoE^{-/-}$ mice were stained using anti-BSAC antibodies (MRTF-A). Oil-red O: Oil-red O staining. Three different experiments gave identical results. (**C**) Real-time RT–PCR analysis showing the relative levels of myocardin mRNA in atherosclerotic aortas from $Mkl1^{-/-}$;$ApoE^{-/-}$ and $Mkl1^{+/+}$;$ApoE^{-/-}$ mice fed a high-cholesterol diet ($n=4$ each). (**D**) Representative images of atherosclerotic lesions from an en-face analysis of the total aorta in $Mkl1^{+/+}$;$ApoE^{-/-}$ and $Mkl1^{-/-}$;$ApoE^{-/-}$ mice fed a high-cholesterol diet. Sudan III staining. Three independent experiments showed identical results. Red colour shows lipid-laden areas representing atherosclerotic lesions. (**E**) Graphs showing the relative (%) area of atherosclerotic lesions in cross-sections of proximal aorta from $Mkl1^{+/+}$;$ApoE^{-/-}$ and $Mkl1^{-/-}$;$ApoE^{-/-}$ mice fed a high-cholesterol diet for 8 weeks ($n=8$ each). *$P<0.05$. (**F**) Representative images of atherosclerotic lesions in cross-sections of proximal aorta from $Mkl1^{+/+}$;$ApoE^{-/-}$ and $Mkl1A^{-/-}$;$ApoE^{-/-}$ mice fed a high-cholesterol diet. Oil-red O: Oil-red O staining. SM-MHC: staining with anti-SM-MHC antibody. Bar indicates 100 μm. All graphs are shown as means ± s.e.m.

Figure 4 MRTF-A mediates acquisition of migration capacity by dedifferentiated VSMCs through regulation of SRF-target genes. (**A**) Real-time RT–PCR analysis showing relative levels of vinculin, MMP9 and integrin β1 mRNAs (normalized to GAPDH mRNA) in femoral arteries 2 weeks after wire injury in $Mkl1^{+/+}$ and $Mkl1^{-/-}$ mice ($n=4$ each). (**B**) Representative western blots showing myocardin, MRTF-A and MRTF-B in arteries 2 weeks after wire injury, in sham-operated arteries and in cultured mouse aortic VSMCs (MAVSMCs) and rat aortic VSMCs (RAVSMCs). (**C**) Real-time RT–PCR analysis showing the relative levels of myocardin, MRTF-A and MRTF-B mRNAs in femoral arteries 2 weeks after wire injury (injury), in sham-operated arteries (sham) and in cultured MAVSMCs and RAVSMCs ($n=6$ each). (**D**) Real-time RT–PCR analysis showing relative levels of MRTF-A, myocardin, vinculin, MMP9 and integrin β1 mRNAs in RAVSMCs transfected with MRTF-A siRNA or control siRNA ($n=6$ each). (**E**) Co-transfection of a plasmid expressing MRTF-A (0, 10 and 100 ng) plus the luciferase reporter gene driven by bp −360 to +63 of the 5′-flanking region of vinculin gene (vinculin-luc) into RAVSMCs (left panel) and NIH3T3 cells (right panel). Relative luciferase activities normalized to Renilla luciferase (pRL-TK) activity are shown. Vinculin CArG-mut-luc: luciferase reporter gene driven by the vinculin promoter harbouring a mutation within the CArG-box. Data were obtained from three experiments performed in sextuplicate. (**F**) Co-transfection of MRTF-A siRNA plus vinculin-luc into RAVSMCs. Relative luciferase activities normalized to Renilla luciferase activity are shown. Data were obtained from two experiments performed in sextuplicate. (**G**) Migration in the presence or absence of PDGF-BB of RAVSMCs transfected with MRTF-A siRNA or control siRNA. Data were obtained from three experiments performed in sextuplicate. (**H**) Proliferation in the presence or absence of fetal calf serum (FCS) of RAVSMCs transfected with MRTF-A siRNA or control siRNA. Data were obtained from three experiments performed in sextuplicate. All graphs are shown as means ± s.e.m. *$P<0.05$ and **$P<0.01$. NS, not significant. Figure source data can be found with the Supplementary data.

F4/80-stained area normalized to the corresponding total atherosclerotic lesion area, did not significantly differ between *Mkl1*$^{+/+}$;*ApoE*$^{-/-}$ and *Mkl1*$^{-/-}$;*ApoE*$^{-/-}$ mice (Supplementary Figure S3B).

MRTF-A is necessary for acquisition of migratory capacity in dedifferentiated VSMCs

SRF controls cellular migration capacity in various cell types, including dedifferentiated VSMCs, by regulating the expres-

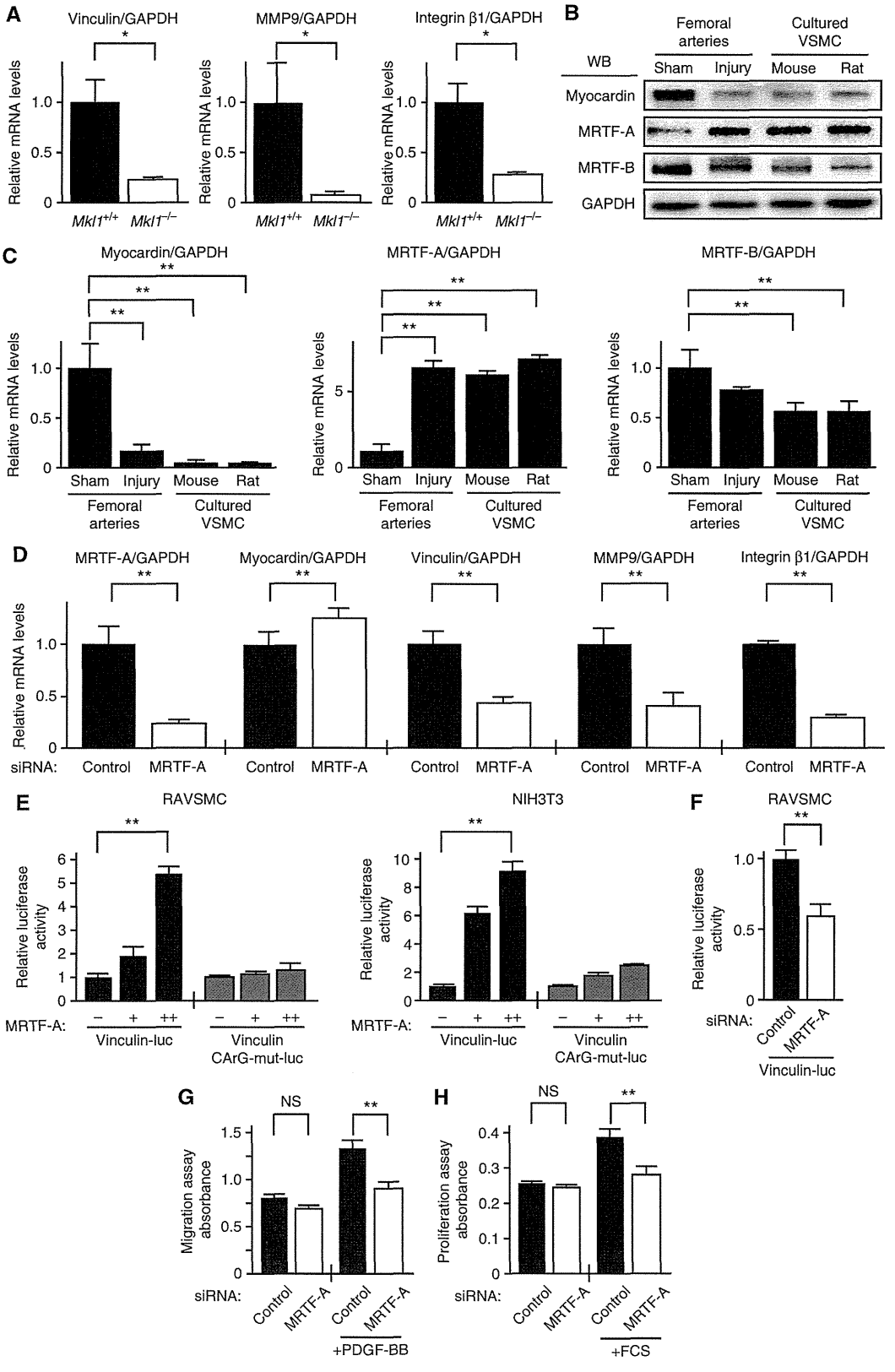

sion of several target genes, including the genes encoding vinculin, MMP9 and integrin β1 (Kenagy *et al*, 1997; Xu *et al*, 1998; Morita *et al*, 2007; Medjkane *et al*, 2009; Olson and Nordheim, 2010). We therefore examined the expression of these SRF-target genes in wire-injured femoral arteries. We found that 2 weeks after wire injury there was significantly less expression of vinculin, MMP9 and integrin β1 genes in the injured femoral arteries of *Mkl1*$^{-/-}$ mice than control *Mkl1*$^{+/+}$ mice (Figure 4A). The expression of these genes in the intact femoral arteries of *Mkl1*$^{-/-}$ and control *Mkl1*$^{+/+}$ mice was not significantly different (Supplementary Figure S4A). The mRNA expression of other SRF targets, αSMA (*ACTA2*) and SM-MHC (*Myh11*) genes encoding smooth muscle-specific contractile proteins, was also significantly less in the injured femoral arteries of *Mkl1*$^{-/-}$ mice than *Mkl1*$^{+/+}$ mice (Supplementary Figure S4B). In primary mouse aortic VSMCs (MAVSMCs), a cellular model of dedifferentiated VSMCs in which MRTF-A expression is increased and myocardin expression is decreased (Figure 4B and C; Supplementary Figure S4C; Hinson *et al*, 2007; Nakamura *et al*, 2010), levels of vinculin, MMP9, integrin β1 and αSMA mRNA were significantly reduced after knocking down MRTF-A (Figure 4D; Supplementary Figure S4D). This suggests that MRTF-A plays a predominant role in maintaining the expression of several SRF-target genes involved in cellular migration in dedifferentiated VSMCs, where expression of myocardin is decreased (Figure 4B and C; Nakamura *et al*, 2010). Overexpression of MRTF-A stimulated vinculin promoter activity in an SRF-dependent manner in both primary rat aortic VSMCs (RAVSMCs) and NIH3T3 fibroblasts (Figure 4E), whereas knocking down MRTF-A reduced vinculin promoter activity in RAVSMCs (Figure 4F). This supports the conclusion that MRTF-A regulates the expression of SRF-target genes in dedifferentiated VSMCs. Furthermore, knocking down MRTF-A significantly impaired PDGF-BB-induced RAVSMC migration, whereas knocking down myocardin did not (Figure 4G; Supplementary Figure S4E and F).

Because SRF is also known to control cellular proliferation, we examined the effect of MRTF-A knockdown on RAVSMC proliferation, and found that knocking down MRTF-A significantly reduced serum-induced RAVSMC proliferation, whereas knocking down myocardin did not (Figure 4H; Supplementary Figure S4G).

Reduced miR-1 expression contributes to the increase in MRTF-A expression in dedifferentiated VSMCs

We next investigated the molecular mechanisms potentially involved in regulating the reciprocal expression of MRTF-A and myocardin during VSMC dedifferentiation. We initially hypothesized that increased expression of myocardin leads to the repression of MRTF-A gene transcription through either direct or indirect mechanisms. Within the MRTF-A gene, the 5′-flanking region (FR) up to 1 kbp from the transcription start site is well conserved among different species. However, we failed to detect any significant effects of myocardin or MRTF-A on the activity of −930 bp MRTF-A promoter region in either RAVSMCs or NIH3T3 cells (Figure 5A; Supplementary Figure S5A). Myocardin also did not significantly affect the promoter activity of −5500 bp MRTF-A promoter region in either RAVSMCs or NIH3T3 cells (Supplementary Figure S5B). We therefore focused on the role of the 3′-untranslated region (UTR) of MRTF-A mRNA, where we found a conserved target site for microRNA-1 (miR-1) (Figure 5B). We observed that expression of miR-1 in vascular tissues is >100 times higher than in several non-muscle tissues, though its expression in skeletal and cardiac muscle tissues is much higher (Figure 5C). Consistent with earlier reports that miR-1 expression is regulated by myocardin and SRF in VSMCs and is downregulated in neointimal lesions created by ligation of carotid arteries of mice (Zhao *et al*, 2005; Chen *et al*, 2011), miR-1 expression was significantly weaker in the injured femoral arteries and atherosclerotic aorta of *ApoE*$^{-/-}$ mice, where there was a corresponding reduction of myocardin expression, than in control arteries (Figures 1A through C and 5D; Supplementary Figure S5C). Levels of miR-1 expression were also substantially lower in cultured RAVSMCs than in normal arteries (Supplementary Figure S5D). Overexpression of a miR-1 mimic significantly reduced endogenous MRTF-A gene and protein expression in RAVSMCs (Figure 5E and F), whereas overexpression of a miR-1 inhibitor significantly increased MRTF-A mRNA and protein expression (Figure 5G and H).

We also assessed miR-1-induced repression of MRTF-A gene by placing its 3′-UTR downstream of a cytomegalovirus (CMV)-driven luciferase reporter and performing luciferase assays in COS7 cells transfected with a miR-1 mimic or control scrambled oligo (Figure 5I). The miR-1 mimic significantly reduced the activity of the luciferase reporter linked to the MRTF-A 3′-UTR, and a mutation in the predicted miR-1 binding site in the 3′-UTR prevented that repression (Figure 5J). Moreover, overexpression of myocardin in A7r5 VSMCs significantly repressed the activity of a luciferase reporter gene linked to the MRTF-A 3′-UTR in a miR-1-dependent fashion (Figure 5K). These results strongly suggest that reduced expression of miR-1 caused by the reduction in myocardin expression during the process of phenotypic modulation of VSMCs contributes to the increase in MRTF-A expression in dedifferentiated VSMCs. Consistent with those findings, injection of an anti-miR-1 Locked Nucleic Acid (LNA)™-enhanced microRNA inhibitor into the injured vessels led to an increase in MRTF-A gene expression and exacerbated the pathological vascular remodelling after wire injury (Supplementary Figure S5E through G; Supplementary Table S2).

Pharmacological inhibition of MRTF-A activity attenuates adverse vascular remodelling after wire injury

The results presented raise the possibility that MRTF-A is a novel therapeutic target for the treatment of vascular disease. Recently, a small molecule (CCG-1423) was found to inhibit Rho pathway-mediated SRF activation (Evelyn *et al*, 2007; Jin *et al*, 2011). CCG-1423 appears to inhibit the interaction between SRF and MRTF-A at a point upstream of the DNA binding. Although the site of inhibition and its selectivity is not yet precisely defined, it was recently shown that CCG-1423 blocks nuclear translocation of MRTF-A, thereby inhibiting MRTF-A-mediated effects on SRF transcription, at least in part (Jin *et al*, 2011). In addition, we confirmed that CCG-1423 blocks serum-induced nuclear accumulation of endogenous MRTF-A in RAVSMCs (Figure 6A). CCG-1423 also significantly blocked SRF activity induced by co-expres-

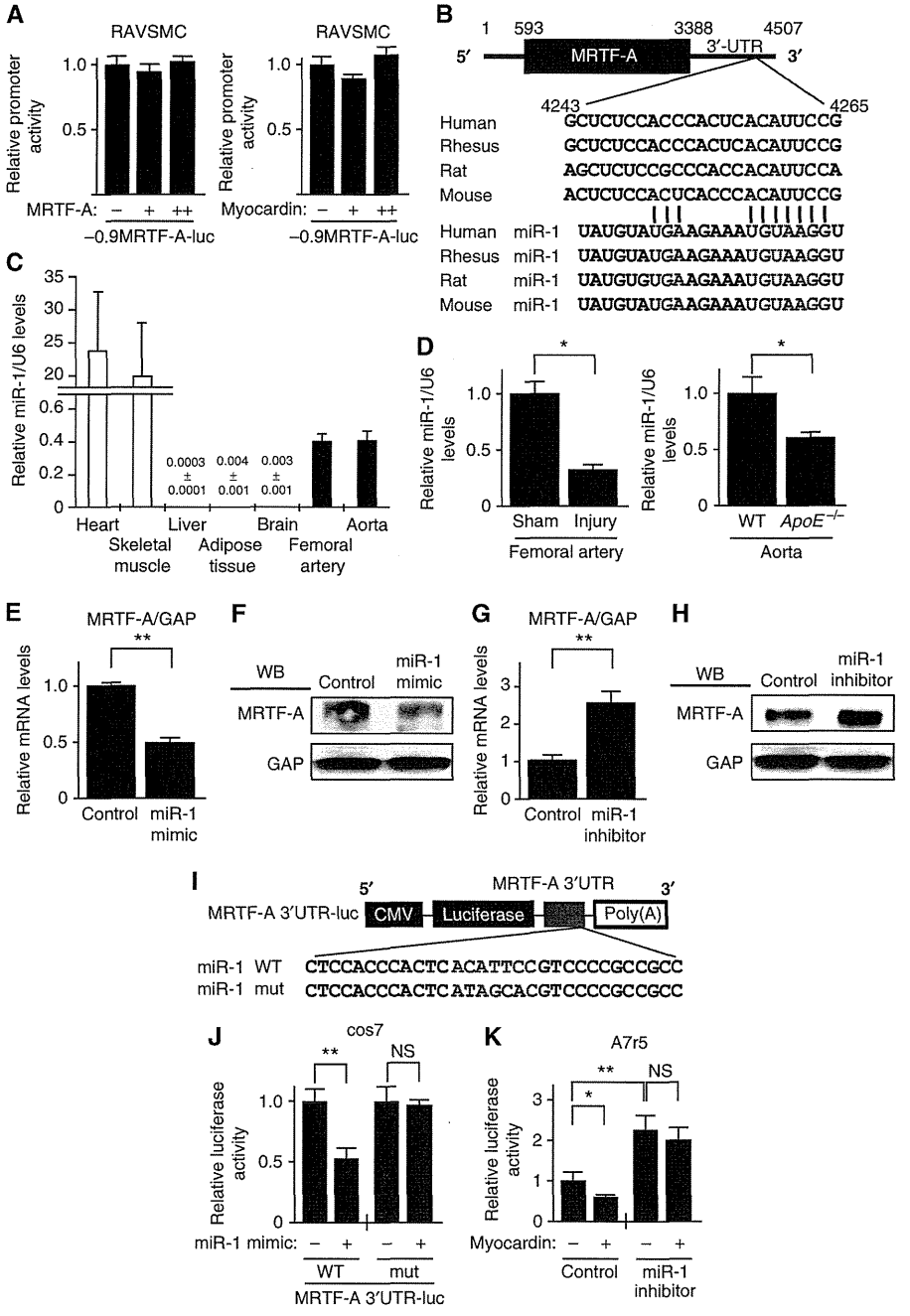

Figure 5 MicroRNA-1 regulates MRTF-A gene expression. (**A**) Co-transfection of a plasmid encoding myocardin or MRTF-A (0, 10 and 100 ng) with the −930 bp MRTF-A-luc gene into RAVSMCs. Data were obtained from two experiments performed in quadruplicate. +: 10 ng. + +: 100 ng. (**B**) Schematic representation of the MRTF-A 3′-untranslated region (UTR) containing a conserved microRNA-1 (miR-1) target site (shown in red). Sequences of mature miR-1 in different species are shown below. (**C**) Real-time RT–PCR analysis showing the relative miR-1 expression (normalized to the U6 levels) in different mouse tissues. (**D**) Real-time RT–PCR analysis showing the relative miR-1 expression (normalized to the U6 levels) in femoral arteries 2 weeks after wire injury or sham operation in wild-type mice ($n=4$ each) (left panel), and in aortic tissues in $ApoE^{-/-}$ or control wild-type mice (right panel). (**E**) Endogenous expression of MRTF-A mRNA in RAVSMCs transfected with miR-1 mimic or control oligo. Graphs show the relative MRTF-A mRNA levels (normalized to GAPDH mRNA) ($n=4$ each). (**F**) Representative western blots showing the effect of miR-1 mimic on MRTF-A expression in RAVSMCs. Three different experiments gave identical results. (**G**) Endogenous MRTF-A mRNA expression in RAVSMCs transfected with miR-1 inhibitor. Graphs show the relative MRTF-A mRNA levels ($n=4$ each). (**H**) Representative western blots showing the effect of a miR-1 inhibitor on MRTF-A expression in RAVSMCs. Three different experiments gave identical results. (**I**) Luciferase reporter constructs containing wild-type and mutant MRTF-A 3′UTR (MRTF-A 3′UTR-luc and mutMRTF-A 3′UTR-luc, respectively). The conserved miR-1 target site is shown in red. In mutMRTF-A 3′UTR-luc, mutations were introduced within the miR-1 target site (shown in blue). (**J**) MRTF-A 3′UTR-luc and mutMRTF-A 3′UTR-luc were co-transfected with miR-1 mimic into COS7 cells for 48 h. Data were obtained from three experiments performed in quadruplicate. (**K**) MRTF-A 3′UTR-luc was transfected with or without a plasmid expressing myocardin and/or a miR-1 inhibitor into A7r5 cells for 48 h. Data were obtained from three experiments performed in quadruplicate. All graphs are shown as means ± s.e.m. Relative luciferase activities normalized to control Renilla luciferase activity are shown. $^{*}P<0.05$. $^{**}P<0.01$. NS, not significant. Figure source data can be found with the Supplementary data.

sion of striated muscle activator of rho signalling (STARS) and MRTF-A in RAVSMCs (Figure 6B; Kuwahara *et al*, 2005). STARS is an actin-binding protein that activates SRF by inducing nuclear accumulation of MRTF-A. Both CCG-1423 and MRTF-A knockdown similarly inhibited STARS-induced activation of SRF in RAVSMCs. Furthermore, this inhibitory effect of CCG-1423 on STARS-induced activation of SRF was abolished by knocking down MRTF-A, supporting the notion that CCG-1423 blocks MRTF-A-mediated activation of SRF (Supplementary Figure S6A) Similarly to knocking down MRTF-A, CCG-1423 significantly reduced the migration and proliferation capacities of RAVSMCs (Figure 6C and D). When we then treated mice subjected to femoral artery wire injury with CCG-1423 (0.15 mg/kg intraperitoneally for 3 weeks), we found that CCG-1423 significantly attenuated the progression of vascular remodelling in arteries 3 weeks after injury (Figure 6E and F; Table II; Supplementary Figure S6B and C), without affecting the hemodynamic parameters or cholesterol profiles (Supplementary Figure S6D and E). CCG-1423 did not affect gross appearance, body weight or survival among the mice during the experiment (data not shown). Furthermore, administration of CCG-1423 also significantly attenuated the

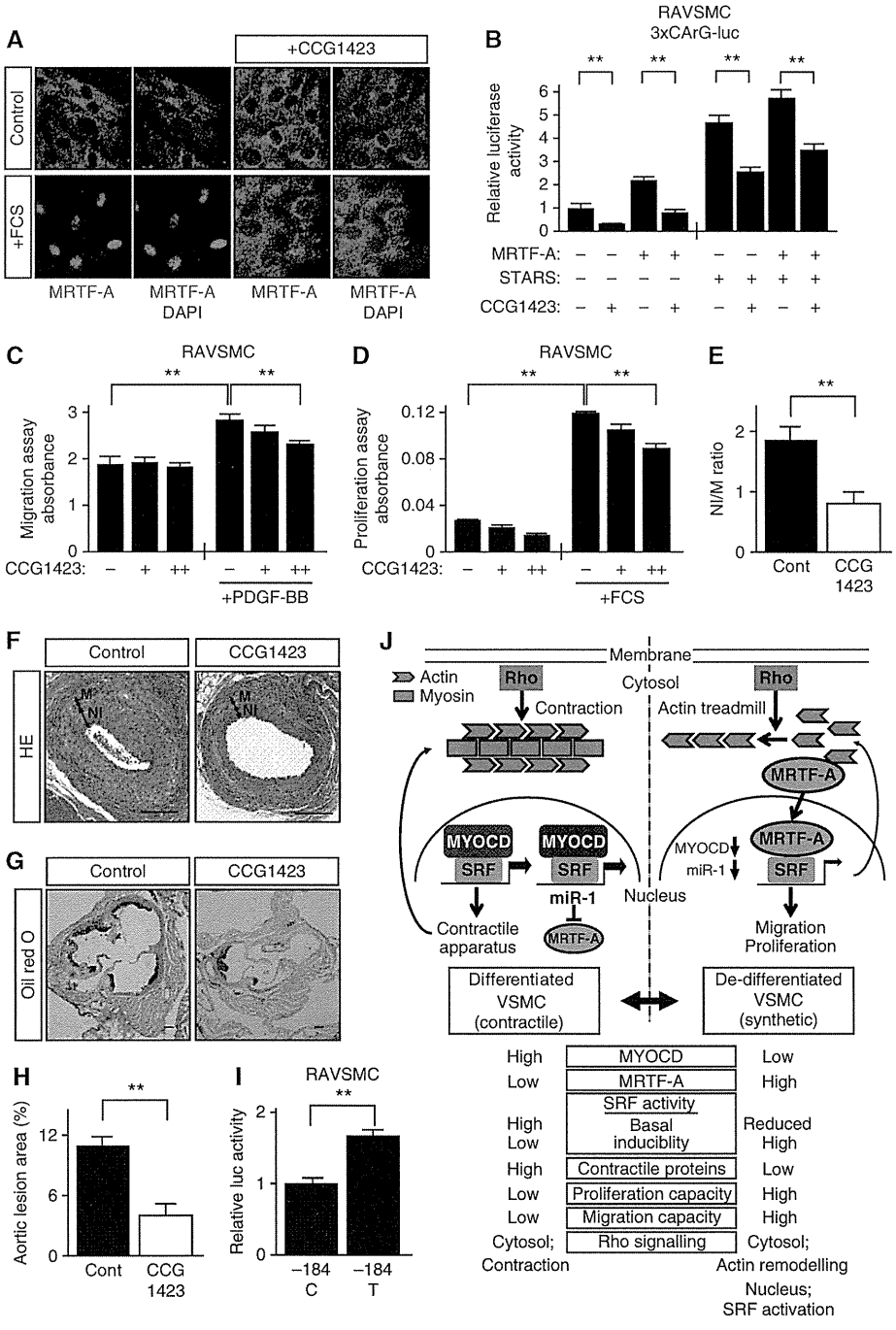

development of atherosclerotic lesions in *ApoE*$^{-/-}$ mice fed a high cholesterol diet for 6 weeks (Figure 6G and H; Supplementary Figure S6F).

Recently, it has been revealed that an SNP in the promoter region of the human MRTF-A gene (−184C>T), which results in a high transcriptional activity in HeLa and K562 cells, is associated with susceptibility to CAD (Hinohara *et al*, 2009). We found that the −930 bp of MRTF-A promoter containing −184T, which is associated with high CAD susceptibility, showed significantly stronger transcriptional activity than the wild-type promoter in cultured RAVSMCs (Figure 6I). These results further support our notion that inhibition of MRTF-A could be an effective novel approach to the treatment and prevention of vascular disorders.

Discussion

In the present study, we used three vascular injury models (femoral artery wire injury, carotid artery ligation and diet-induced atherosclerosis in *APOE*$^{-/-}$ mice) in *Mkl1*$^{-/-}$ mice to elucidate the roles played by MRTF-A in pathological vascular remodelling. We initially found that expression of MRTF-A mRNA and protein was significantly increased in injured arteries and aortic tissues containing atherosclerotic lesions in *ApoE*$^{-/-}$ mice, while expression of myocardin was reciprocally decreased. In each model, neointima formation or atherosclerotic lesions were significantly smaller in *Mkl1*$^{-/-}$ mice than in the respective controls. The expression of vinculin, MMP-9 and integrin β1 genes, which are targets of SRF and key regulators of cellular migration, was significantly diminished in the injured arteries of *Mkl1*$^{-/-}$ mice. Knocking down MRTF-A in RAVSMCs reduced expression of these genes in response to extracellular stimuli, which significantly impaired cell migration. These results demonstrate that induced expression of MRTF-A is crucial for acquisition of the capacity to migrate in response to environmental stress in dedifferentiated VSMCs (Liu *et al*, 2005). We also found that MRTF-A gene expression in VSMCs is, at least in part, regulated by miR-1, which is in turn regulated by myocardin and SRF (Jiang *et al*, 2010; Chen *et al*, 2011). Expression of miR-1 was reduced in dedifferentiated VSMCs, along with that of myocardin. This apparently led to an increase in MRTF-A expression, though it is possible that another as yet unidentified mechanism, such as transcriptional regulation through sites located in the distal 5′-FR or within introns, also contribute to the reciprocal regulation of myocardin and MRTF-A expression. Finally, we showed that a small molecule inhibitor of MRTF-A, CCG-1423, significantly reduced neointima formation following wire injury to mouse femoral arteries. Collectively, these results demonstrate that induction of MRTF-A plays a key role in vascular remodelling by maintaining SRF activity, thereby conferring a capacity for migration in response to extracellular stimuli on dedifferentiated VSMCs. MRTF-A is thus a potentially useful therapeutic target that may be more specific and efficient than the upstream Rho family GTPases, which can affect diverse intracellular signalling events.

In differentiated VSMCs, myocardin strongly activates SRF and the expression of VSMC-specific contractile proteins, thereby contributing to the maintenance of the contractile phenotype (Wang *et al*, 2003). Myocardin is constitutively located in the nucleus, where it suppresses MRTF-A expression via activation of miR-1. The ability of MRTF-B to transduce Rho signalling into the nucleus is much weaker than that of MRTF-A (Kuwahara *et al*, 2005; Nakamura *et al*, 2010),

Table II Luminal and neointimal area of femoral arteries 3weeks after vascular injury

	n	Lumen ($\times 10^3/\mu m^2$)	Intima ($\times 10^3/\mu m^2$)	Media ($\times 10^3/\mu m^2$)	IEL ($\times 10^3/\mu m^2$)	EEL ($\times 10^3/\mu m^2$)	Intima/Media ratio
Control injury	6	15.0±3.0	39.9±4.1	22.9±2.1	55.0±2.4	77.8±3.7	1.85±0.17
CCG1423 injury	8	22.3±5.6	20.2±4.8*	24.8±1.6	43.0±7.2	67.8±2.8	0.81±0.19*

The ratio of intima to media was calculated as the intimal area/medial area. Values are means±s.e.m. IEL, internal elastic lamina; EEL, external elastic lamina. *$P<0.01$ versus control injured arteries.

Figure 6 CCG-1423, an MRTF-A inhibitor, attenuated neointima formation induced by wire injury in mouse femoral arteries. (**A**) CCG-1423 diminished the nuclear accumulation of endogenous MRTF-A induced by 20% FCS in RAVSMCs. Cells were stained with anti-MRTF-A antibody (green) and DAPI (blue). (**B**) CCG-1423 significantly inhibited MRTF-A-induced SRF activity in RAVSMCs. Graphs show the relative luciferase activities of 3 × CArG-luc. STARS: expression plasmid encoding striated muscle activator of Rho signalling. Data were obtained from two experiments performed in quintuplicate. (**C**) PDGF-BB-induced migration was assessed in RAVSMCs treated without or with 0.1 μm (+) or 1 μm (++) of CCG-1423. Data were obtained from two experiments performed in sextuplicate. (**D**) FCS-induced proliferation was assessed in RAVSMCs treated without or with 0.1 μm (+) or 1 μm (++) of CCG-1423. Data were obtained from two experiments performed in quadruplicate. (**E, F**) Effect of CCG-1423 on neointima formation in wire-injured femoral arteries in mice. Graph showing the neointima (NI)-to-media (M) ratio in wire-injured arteries from mice treated without (control) or with CCG-1423 ($n=3$ in control group and 4 in CCG1423 group) (**E**). Representative images of neointima are shown (**F**). (**G**) Representative images of atherosclerotic lesions in cross-sections of proximal aorta from *ApoE*$^{-/-}$ mice fed a high-cholesterol diet with or without CCG-1423 for 6 weeks. Oil-red O: Oil-red O staining. Bar indicates 100 μm. (**H**) Graphs showing the relative (%) area of atherosclerotic lesions in cross-sections of proximal aorta from *ApoE*$^{-/-}$ mice fed a high-cholesterol diet and treated with or without CCG-1423 for 6 weeks ($n=3$ in control group and 4 in CCG-1423 group). **$P<0.01$. (**I**) Effect of an SNP in the promoter region of MRTF-A gene (−184C>T) on the promoter activity in RAVSMCs. Relative activities of −930 bp MRTF-A(−184C)-luc and −930 bp MRTF-A(−184T)-luc in two different experiments performed in quadruplicate are shown. All graphs are shown as means±s.e.m. **$P<0.01$. (**J**) A proposed model of the role of MRTF-A in vascular remodelling. In differentiated, contractile VSMCs, constitutively nuclear myocardin strongly activates SRF, leading to expression of VSMC-specific contractile proteins, and suppresses MRTF-A expression through activation of miR-1. Under these conditions, cytosolic Rho signalling is confined almost exclusively to regulation of contraction. In dedifferentiated VSMCs, MRTF-A expression is induced by reductions in miR-1 expression and basal SRF activity, thereby maintaining the lower basal SRF activity necessary for cellular migration and proliferation. Because MRTF-A is shuttled between the cytosol and nucleus and because it activates SRF downstream of Rho signalling, in dedifferentiated VSMCs, extracellular stimuli activating Rho signalling can substantively affect cellular proliferation and migration by modulating SRF activity. MYOCD: myocardin.

so that Rho family signalling is almost exclusively confined to regulating contraction through modifying Ca^{2+} sensitivity in the cytosol. By contrast, in dedifferentiated synthetic VSMCs, the reduction in myocardin expression leads to a reduction in basal SRF activity and then to a loss of VSMC-specific contractile components. Under these conditions, MRTF-A expression is induced, at least in part, by the reduction in miR-1 also caused by diminished myocardin, and is sufficient to maintain the SRF activity necessary for cellular migration and proliferation. Because MRTF-A is shuttled between the cytosol and nucleus, where it activates SRF downstream of Rho family GTPase-actin signalling, in dedifferentiated VSMCs extracellular stimuli activating Rho GTPase signalling can substantively affect cellular proliferation and migration by modulating SRF activity (Medjkane *et al*, 2009; Olson and Nordheim, 2010). Loss or inhibition of MRTF-A reduced stimulus-induced cell migration and proliferation, making cells static (Figure 6J). This suggests that the reciprocal expression of MRTF-A and myocardin mediated by miR-1 regulates the plasticity of effectors downstream of Rho family signalling, thereby contributing to phenotypic modulation of VSMC during vascular remodelling.

In addition to the classical concept that dedifferentiated intimal VSMCs are derived from medial VSMCs, recent evidence raises the possibility that VSMC progenitor cells in the circulation or adventitia also contribute to intimal VSMCs (Sata *et al*, 2002; Hoglund *et al*, 2010). We have not addressed the role of MRTF-A in the process of intimal VSMC differentiation from such progenitor cells in this study. In that context, however, MRTF-A has been shown to be involved in the differentiation of mesenchymal stem cells into VSMCs (Jeon *et al*, 2008). Thus, MRTF-A may also play an important role in the molecular processes underlying migration, proliferation and differentiation of VSMC progenitor cells into intimal VSMCs during vascular remodelling.

Recently, human genetic screening to identify novel susceptibility loci for CAD using microsatellite markers and SNP analysis revealed that an SNP in the promoter region of the MRTF-A gene (−184C>T) is associated with susceptibility to CAD (Hinohara *et al*, 2009). Moreover, functional analysis suggested that heightened MRTF-A expression is associated with increased susceptibility to CAD. We observed that the MRTF-A promoter containing −184T, which is associated with high CAD susceptibility, showed significantly stronger transcriptional activity than the wild-type promoter in cultured VSMCs (Figure 6I). These observations further support the conclusion that MRTF-A is crucially involved in pathological vascular remodelling underlying the development of vascular diseases, and imply that MRTF-A is a potentially useful therapeutic target for prevention of the progression of vascular diseases.

Materials and methods

Plasmids

−930 bp MRTF-A(−184C)-luc (MRTF-A-luc), vinculin-luc, vinculin CArG-mut-luc and 3 × CArG-luc were described previously (Kuwahara *et al*, 2007; Morita *et al*, 2007; Hinohara *et al*, 2009). Expression vectors used in the experiments were described previously (Kuwahara *et al*, 2007). MRTF-A 3′UTR-luc and mutMRTF-A 3′UTR-luc were respectively generated by inserting the MRTF-A 3′UTR containing wild type or mutated miR-1 target sequences downstream of the luciferase gene in a pMIR-REPORTER kit miRNA reporter expression vector (Ambion). −5500 bp MRTF-A-luc was generated by inserting 5500 bp of the 5′-FR of MRTF-A gene upstream of the luciferase gene in pGL4 vector (Promega).

Animal experiments

MRTF-A$^{-/-}$ mice were kindly provided from Dr EN Olson (The University of Texas, Southwestern Medical Center at Dallas) (Li *et al*, 2006). *ApoE*$^{-/-}$ and *MRTF-A*$^{-/-}$ mice (C57BL/6 background) were cross-bred (Kobayashi *et al*, 2004; Li *et al*, 2006). The animal care and all experimental protocols were reviewed and approved by the Animal Research Committee at Kyoto University Graduate School of Medicine.

Cell culture and transfection

RAVSMCs (Cell Applications. Inc.), A7r5 (DS Pharma Biomedical), NIH3T3 and COS7 cells were maintained in DMEM supplemented with 10% FCS. Co-transfection of RAVSMCs with 3 × CArG-luc plus expression plasmids encoding MRTF-A (1 ng) and STARS (100 ng), or with MRTF-A-luc plus expression plasmids encoding myocardin and MRTF-A (0, 1 or 10 ng each) was accomplished using FuGene6 (Roche). pRL-TK (Roche) was included in all transfections as an internal control. MiRIDIAN microRNA mimic for miR-1, miRIDIAN microRNA hairpin inhibitor for miR-1 or a negative control for each (Thermo Scientific) was transfected into RAVSMCs grown in 6-cm dishes using Dharmafect2. MAVSMCs were obtained as previously reported (Nakamura *et al*, 2010).

RNA interference

RAVSMCs grown in 6-cm dishes were transfected with 200 pmol of ON-TARGET plus® siRNA reagent targeting rat MRTF-A or myocardin, or control scrambled siRNA (Thermo Scientific) using Dharmafect 2. For luciferase assays, RAVSMCs grown in 24-well dishes were transfected with 100 pmol of siRNA and 500 ng of luciferase reporter plasmid using Fugene 6.

Mouse vascular injury

Vascular wire injury was induced in femoral arteries of male C57BL/6 wild-type or *Mkl1*$^{-/-}$ mice at 8–10 weeks of age, as described previously (Sata *et al*, 2000; Takaoka *et al*, 2009). LNA oligonucleotide anti-miR-1 microRNA inhibitor or LNA microRNA inhibitor negative control (20 mg/kg) (5′-FAM prelabelled, Exiqon) was injected into sham-operated or injured femoral arteries from the muscular branch using a syringe with 29 gauge needle (TERUMO).

Quantification of neointimal hyperplasia

We harvested the femoral and carotid arteries 4 weeks after wire injury, unless otherwise indicated. Digitalized images were analysed using image analysis software (Image J, NIH), and the intimal and medial areas were recorded. The average of the neointima/media ratios in FIVE serial sections was designated as the value to represent each individual.

Analysis of atherosclerotic lesion area in ApoE$^{-/-}$ mice

Mkl1$^{+/+}$;*ApoE*$^{-/-}$ and *Mkl1A*$^{-/-}$;*ApoE*$^{-/-}$ mice were fed normal chow for 4 weeks beginning when the mice were 4 weeks old. Then beginning when they were 8 weeks old, they were fed a high-cholesterol diet (F2HFD1, Oriental Biotechnology) for 8 weeks. Atherosclerotic lesions were analysed by en-face analysis of the whole aorta and quantified by cross-sectional analysis of the proximal aorta, as described previously (Paigen *et al*, 1987; Palinski *et al*, 1994; Kobayashi *et al*, 2004).

Immunohistochemical analysis

Paraffin-embedded sections (4 μm thick) of femoral arteries harvested 4 weeks after wire injury were stained with anti-Mac3, anti-CD31, mouse monoclonal anti-αSMA (Sigma-Aldrich), rabbit polyclonal anti-SM-MHC (BT-562, Biomedical Technologies Inc.) or anti-BSAC antibodies (Sasazuki *et al*, 2002). Ratios of total numbers of Mac-3-positive cells in the intima and the media and CD31-positive endothelial cells in *Mkl1*$^{+/+}$ and *Mkl1*$^{-/-}$ mice were quantified ($n=4$ and 5 in each group, respectively). Sections of proximal aortas from *ApoE*$^{-/-}$ mice were stained with anti-α-SMA, anti-SM-MHC or anti-BSAC antibody.

Real-time RT–PCR

Real-time one-step RT–PCR was performed using One-step RT-PCR master mix reagent (Applied Biosystems). MiR-1 expression was determined using a Taqman MicroRNA RT kit and Taqman Universal PCR Master Mix II (Applied Biosystems). All taqman primers and probes were purchased from Applied Biosystems.

Western blot analysis

Western blot analysis was performed using rabbit polyclonal anti-myocardin, anti-MRTF-A and anti-MRTF-B antibodies as described previously (Kuwahara *et al*, 2005; Nakamura *et al*, 2010).

Statistical analysis

Data are presented as means ± s.e.m. Unpaired *t*-tests were used for comparison between two groups, and ANOVA with *post hoc* Fisher's test was used for comparison among groups. Values of $P<0.05$ were considered as significant. Data obtained from the two-way factorial design were analysed with the two-way ANOVA.

Supplementary data

Supplementary data are available at *The EMBO Journal* Online (http://www.embojournal.org).

Acknowledgements

We thank H Yanagisawa (The University of Texas Southwestern Medical Center at Dallas), T Murayama, H Arai, E Ashihara and T Maekawa (Kyoto University) for their technical instruction; Y Kubo for her excellent secretarial work; K Hinohara (Tokyo Medical and Dental University) for preparation of MRTF-A-luciferase constructs; and F Kataoka, A Fujishima and A Abe for their excellent technical assistance. We also gratefully thank EN Olson and R Bassel-Duby (The University of Texas Southwestern Medical Center at Dallas) for providing us MRTF-A knockout mice. This research was supported by Grants-in-Aid for Scientific Research from the Japan Society for the Promotion of Science (to KK, AK and K N); a grant from the Japanese Ministry of Health, Labour and Welfare (to KN); grants from the Japan Foundation for Applied Enzymology, the Mitsubishi Pharma Research Foundation, the Astellas Foundation for Research on Metabolic Disorders, the Vehicle Racing Commemorative Foundation, the Takeda Medical Research Foundation, the Takeda Science Foundation, the Hoh-ansha Foundation, the SENSHIN Medical Research Foundation (to KK) and the Kimura Memorial Heart Foundation (to HK).

Author Contributions: TM conducted most of the experiments and contributed to data analysis. KK and NK conceived of and directed the project. MT, HK, YK, MS, TS and RN provided technical help on animal experiments. YN, HN, TN, KS and AK performed some experiments using luciferase reporter assays, immunohistochemical analysis and western blot analysis with TM. KN, YY, CY, JS, SU, TN and YK contributed to data analysis.

Conflict of interest

The authors declare that they have no conflict of interest.

References

Bentzon JF, Weile C, Sondergaard CS, Hindkjaer J, Kassem M, Falk E (2006) Smooth muscle cells in atherosclerosis originate from the local vessel wall and not circulating progenitor cells in ApoE knockout mice. *Arterioscler Thromb Vasc Biol* **26:** 2696–2702

Chen J, Yin H, Jiang Y, Radhakrishnan SK, Huang ZP, Li J, Shi Z, Kilsdonk EP, Gui Y, Wang DZ, Zheng XL (2011) Induction of microRNA-1 by myocardin in smooth muscle cells inhibits cell proliferation. *Arterioscler Thromb Vasc Biol* **31:** 368–375

Daniel JM, Bielenberg W, Stieger P, Weinert S, Tillmanns H, Sedding DG (2010) Time-course analysis on the differentiation of bone marrow-derived progenitor cells into smooth muscle cells during neointima formation. *Arterioscler Thromb Vasc Biol* **30:** 1890–1896

Evelyn CR, Wade SM, Wang Q, Wu M, Iniguez-Lluhi JA, Merajver SD, Neubig RR (2007) CCG-1423: a small-molecule inhibitor of RhoA transcriptional signaling. *Mol Cancer Ther* **6:** 2249–2260

Glass CK, Witztum JL (2001) Atherosclerosis. The road ahead. *Cell* **104:** 503–516

Hinohara K, Nakajima T, Yasunami M, Houda S, Sasaoka T, Yamamoto K, Lee BS, Shibata H, Tanaka-Takahashi Y, Takahashi M, Arimura T, Sato A, Naruse T, Ban J, Inoko H, Yamada Y, Sawabe M, Park JE, Izumi T, Kimura A (2009) Megakaryoblastic leukemia factor-1 gene in the susceptibility to coronary artery disease. *Hum Genet* **126:** 539–547

Hinson JS, Medlin MD, Lockman K, Taylor JM, Mack CP (2007) Smooth muscle cell-specific transcription is regulated by nuclear localization of the myocardin-related transcription factors. *Am J Physiol Heart Circ Physiol* **292:** H1170–H1180

Hoglund VJ, Dong XR, Majesky MW (2010) Neointima formation: a local affair. *Arterioscler Thromb Vasc Biol* **30:** 1877–1879

Jeon ES, Park WS, Lee MJ, Kim YM, Han J, Kim JH (2008) A Rho kinase/myocardin-related transcription factor-A-dependent mechanism underlies the sphingosylphosphorylcholine-induced differentiation of mesenchymal stem cells into contractile smooth muscle cells. *Circ Res* **103:** 635–642

Jiang Y, Yin H, Zheng XL (2010) MicroRNA-1 inhibits myocardin-induced contractility of human vascular smooth muscle cells. *J Cell Physiol* **225:** 506–511

Jin W, Goldfine AB, Boes T, Henry RR, Ciaraldi TP, Kim EY, Emecan M, Fitzpatrick C, Sen A, Shah A, Mun E, Vokes V, Schroeder J, Tatro E, Jimenez-Chillaron J, Patti ME (2011) Increased SRF transcriptional activity in human and mouse skeletal muscle is a signature of insulin resistance. *J Clin Invest* **121:** 918–929

Kenagy RD, Hart CE, Stetler-Stevenson WG, Clowes AW (1997) Primate smooth muscle cell migration from aortic explants is mediated by endogenous platelet-derived growth factor and basic fibroblast growth factor acting through matrix metalloproteinases 2 and 9. *Circulation* **96:** 3555–3560

Kobayashi T, Tahara Y, Matsumoto M, Iguchi M, Sano H, Murayama T, Arai H, Oida H, Yurugi-Kobayashi T, Yamashita JK, Katagiri H, Majima M, Yokode M, Kita T, Narumiya S (2004) Roles of thromboxane A(2) and prostacyclin in the development of atherosclerosis in apoE-deficient mice. *J Clin Invest* **114:** 784–794

Kuwahara K, Barrientos T, Pipes GC, Li S, Olson EN (2005) Muscle-specific signaling mechanism that links actin dynamics to serum response factor. *Mol Cell Biol* **25:** 3173–3181

Kuwahara K, Teg Pipes GC, McAnally J, Richardson JA, Hill JA, Bassel-Duby R, Olson EN (2007) Modulation of adverse cardiac remodeling by STARS, a mediator of MEF2 signaling and SRF activity. *J Clin Invest* **117:** 1324–1334

Li S, Chang S, Qi X, Richardson JA, Olson EN (2006) Requirement of a myocardin-related transcription factor for development of mammary myoepithelial cells. *Mol Cell Biol* **26:** 5797–5808

Li S, Wang DZ, Wang Z, Richardson JA, Olson EN (2003) The serum response factor coactivator myocardin is required for vascular smooth muscle development. *Proc Natl Acad Sci USA* **100:** 9366–9370

Liu Y, Sinha S, McDonald OG, Shang Y, Hoofnagle MH, Owens GK (2005) Kruppel-like factor 4 abrogates myocardin-induced activation of smooth muscle gene expression. *J Biol Chem* **280:** 9719–9727

Medjkane S, Perez-Sanchez C, Gaggioli C, Sahai E, Treisman R (2009) Myocardin-related transcription factors and SRF are required for cytoskeletal dynamics and experimental metastasis. *Nat Cell Biol* **11:** 257–268

Miano JM (2003) Serum response factor: toggling between disparate programs of gene expression. *J Mol Cell Cardiol* **35:** 577–593

Miralles F, Posern G, Zaromytidou AI, Treisman R (2003) Actin dynamics control SRF activity by regulation of its coactivator MAL. *Cell* **113:** 329–342

Morita T, Mayanagi T, Sobue K (2007) Reorganization of the actin cytoskeleton via transcriptional regulation of cytoskeletal/focal adhesion genes by myocardin-related transcription factors (MRTFs/MAL/MKLs). *Exp Cell Res* **313:** 3432–3445

Nakamura S, Hayashi K, Iwasaki K, Fujioka T, Egusa H, Yatani H, Sobue K (2010) Nuclear import mechanism for myocardin family

members and their correlation with vascular smooth muscle cell phenotype. *J Biol Chem* **285:** 37314–37323

Nishimura G, Manabe I, Tsushima K, Fujiu K, Oishi Y, Imai Y, Maemura K, Miyagishi M, Higashi Y, Kondoh H, Nagai R (2006) DeltaEF1 mediates TGF-beta signaling in vascular smooth muscle cell differentiation. *Dev Cell* **11:** 93–104

Olson EN, Nordheim A (2010) Linking actin dynamics and gene transcription to drive cellular motile functions. *Nat Rev Mol Cell Biol* **11:** 353–365

Owens GK, Kumar MS, Wamhoff BR (2004) Molecular regulation of vascular smooth muscle cell differentiation in development and disease. *Physiol Rev* **84:** 767–801

Paigen B, Morrow A, Holmes PA, Mitchell D, Williams RA (1987) Quantitative assessment of atherosclerotic lesions in mice. *Atherosclerosis* **68:** 231–240

Palinski W, Ord VA, Plump AS, Breslow JL, Steinberg D, Witztum JL (1994) ApoE-deficient mice are a model of lipoprotein oxidation in atherogenesis. Demonstration of oxidation-specific epitopes in lesions and high titers of autoantibodies to malondialdehyde-lysine in serum. *Arterioscler Thromb* **14:** 605–616

Sasazuki T, Sawada T, Sakon S, Kitamura T, Kishi T, Okazaki T, Katano M, Tanaka M, Watanabe M, Yagita H, Okumura K, Nakano H (2002) Identification of a novel transcriptional activator, BSAC, by a functional cloning to inhibit tumor necrosis factor-induced cell death. *J Biol Chem* **277:** 28853–28860

Sata M, Maejima Y, Adachi F, Fukino K, Saiura A, Sugiura S, Aoyagi T, Imai Y, Kurihara H, Kimura K, Omata M, Makuuchi M, Hirata Y, Nagai R (2000) A mouse model of vascular injury that induces rapid onset of medial cell apoptosis followed by reproducible neointimal hyperplasia. *J Mol Cell Cardiol* **32:** 2097–2104

Sata M, Saiura A, Kunisato A, Tojo A, Okada S, Tokuhisa T, Hirai H, Makuuchi M, Hirata Y, Nagai R (2002) Hematopoietic stem cells differentiate into vascular cells that participate in the pathogenesis of atherosclerosis. *Nat Med* **8:** 403–409

Schwartz SM, deBlois D, O'Brien ER (1995) The intima. Soil for atherosclerosis and restenosis. *Circ Res* **77:** 445–465

Shoji M, Sata M, Fukuda D, Tanaka K, Sato T, Iso Y, Shibata M, Suzuki H, Koba S, Geshi E, Katagiri T (2004) Temporal and spatial characterization of cellular constituents during neointimal hyperplasia after vascular injury: Potential contribution of bone-marrow-derived progenitors to arterial remodeling. *Cardiovasc Pathol* **13:** 306–312

Sun Y, Boyd K, Xu W, Ma J, Jackson CW, Fu A, Shillingford JM, Robinson GW, Hennighausen L, Hitzler JK, Ma Z, Morris SW (2006) Acute myeloid leukemia-associated Mkl1 (Mrtf-a) is a key regulator of mammary gland function. *Mol Cell Biol* **26:** 5809–5826

Takaoka M, Nagata D, Kihara S, Shimomura I, Kimura Y, Tabata Y, Saito Y, Nagai R, Sata M (2009) Periadventitial adipose tissue plays a critical role in vascular remodeling. *Circ Res* **105:** 906–911

Wang D, Chang PS, Wang Z, Sutherland L, Richardson JA, Small E, Krieg PA, Olson EN (2001) Activation of cardiac gene expression by myocardin, a transcriptional cofactor for serum response factor. *Cell* **105:** 851–862

Wang DZ, Li S, Hockemeyer D, Sutherland L, Wang Z, Schratt G, Richardson JA, Nordheim A, Olson EN (2002) Potentiation of serum response factor activity by a family of myocardin-related transcription factors. *Proc Natl Acad Sci USA* **99:** 14855–14860

Wang Z, Wang DZ, Pipes GC, Olson EN (2003) Myocardin is a master regulator of smooth muscle gene expression. *Proc Natl Acad Sci USA* **100:** 7129–7134

Watanabe N, Kurabayashi M, Shimomura Y, Kawai-Kowase K, Hoshino Y, Manabe I, Watanabe M, Aikawa M, Kuro-o M, Suzuki T, Yazaki Y, Nagai R (1999) BTEB2, a Kruppel-like transcription factor, regulates expression of the SMemb/Nonmuscle myosin heavy chain B (SMemb/NMHC-B) gene. *Circ Res* **85:** 182–191

Xu W, Baribault H, Adamson ED (1998) Vinculin knockout results in heart and brain defects during embryonic development. *Development* **125:** 327–337

Zhao Y, Samal E, Srivastava D (2005) Serum response factor regulates a muscle-specific microRNA that targets Hand2 during cardiogenesis. *Nature* **436:** 214–220

http://www.kidney-international.org

Pleiotrophin triggers inflammation and increased peritoneal permeability leading to peritoneal fibrosis

Hideki Yokoi[1,2], Masato Kasahara[1,2], Kiyoshi Mori[1], Yoshihisa Ogawa[1], Takashige Kuwabara[1], Hirotaka Imamaki[1], Tomoko Kawanishi[1], Kenichi Koga[1], Akira Ishii[1], Yukiko Kato[1], Keita P. Mori[1], Naohiro Toda[1], Shoko Ohno[1], Hisako Muramatsu[3], Takashi Muramatsu[4], Akira Sugawara[1], Masashi Mukoyama[1] and Kazuwa Nakao[1]

[1]Department of Medicine and Clinical Science, Kyoto University Graduate School of Medicine, Kyoto, Japan; [2]Division of Nephrology and Blood Purification, Kobe Institute of Biomedical Research and Innovation, Hyogo, Japan; [3]Department of Health and Nutrition, Faculty of Psychological and Physical Science, Aichi Gakuin University, Aichi, Japan and [4]Department of Health Science, Faculty of Psychological and Physical Science, Aichi Gakuin University, Aichi, Japan

Long-term peritoneal dialysis induces peritoneal fibrosis with submesothelial fibrotic tissue. Although angiogenesis and inflammatory mediators are involved in peritoneal fibrosis, precise molecular mechanisms are undefined. To study this, we used microarray analysis and compared gene expression profiles of the peritoneum in control and chlorhexidine gluconate (CG)-induced peritoneal fibrosis mice. One of the 43 highly upregulated genes was pleiotrophin, a midkine family member, the expression of which was also upregulated by the solution used to treat mice by peritoneal dialysis. This growth factor was found in fibroblasts and mesothelial cells within the underlying submesothelial compact zones of mice, and in human peritoneal biopsy samples and peritoneal dialysate effluent. Recombinant pleiotrophin stimulated mitogenesis and migration of mouse mesothelial cells in culture. We found that in wild-type mice, CG treatment increased peritoneal permeability (measured by equilibration), increased mRNA expression of TGF-β1, connective tissue growth factor and fibronectin, TNF-α and IL-1β expression, and resulted in infiltration of CD3-positive T cells, and caused a high number of Ki-67-positive proliferating cells. All of these parameters were decreased in peritoneal tissues of CG-treated pleiotrophin-knockout mice. Thus, an upregulation of pleiotrophin appears to play a role in fibrosis and inflammation during peritoneal injury.

Kidney International (2012) **81,** 160–169; doi:10.1038/ki.2011.305; published online 31 August 2011

KEYWORDS: continuous ambulatory peritoneal dialysis; microarray analysis; peritoneal dialysis; peritoneal membrane

Correspondence: *Masato Kasahara, Department of Medicine and Clinical Science, Kyoto University Graduate School of Medicine, 54 Shogoin Kawahara-cho, Sakyo-ku, Kyoto 606-8507, Japan.*
E-mail: kasa@kuhp.kyoto-u.ac.jp

Received 8 December 2010; revised 19 June 2011; accepted 5 July 2011; published online 31 August 2011

Continuous ambulatory peritoneal dialysis (PD) is a preferred method of home dialysis for patients with end-stage renal failure.[1] Long-term use of PD induces peritoneal fibrosis characterized with the presence of submesothelial fibrotic tissue and increased peritoneal vascularization with vasculopathy.[2] Peritoneal fibrosis occurs in long-term continuous ambulatory PD patients in response to a variety of injuries, including bioincompatible dialysate solutions, peritonitis, uremia, and chronic inflammation.[2,3] Previous reports show that several profibrotic and proinflammatory mediators are upregulated upon induction of peritoneal fibrosis, such as transforming growth factor-β (TGF-β) and interleukin-6 (IL-6).[4–6] Although proinflammatory, angiogenic, and profibrotic cytokines such as IL-1β, vascular endothelial growth factor, and TGF-β are presumed to be involved in the pathogenesis, precise molecular mechanisms that lead to peritoneal sclerosis and encapsulating peritoneal sclerosis are still elusive.[7–9] To identify the novel genes possibly involved in the development of peritoneal fibrosis, we compared gene expression profiles of the peritoneum in chlorhexidine gluconate (CG)-induced peritoneal fibrosis and control mice using microarray.

Microarray analysis is a powerful tool to identify novel genes and pathways involved in the development of peritoneal fibrosis. Although a few papers report microarray analysis for endothelial cells in rat peritoneal dialysate infusion model,[10] analysis for whole mouse gene sets over 39,000 transcripts has not been investigated yet. In this study, we performed microarray analysis using a mouse model of peritoneal fibrosis and selected the genes that changed greatly in peritoneal fibrosis and those that were also present in mesothelial cells. This approach can allow us to specify the genes associated with peritoneal injury.

Here we show that one of the highly upregulated secreted proteins during the development of peritoneal fibrosis is pleiotrophin (PTN). PTN is an 18-kDa secreted protein, belonging to the midkine family and has functions similar to

midkine.[11] The receptors for PTN are the receptor protein tyrosine phosphatase β/ζ (RPTPβ/ζ), anaplastic lymphoma tyrosine kinase (ALK), and syndecan-3.[12] PTN has been shown to promote cell growth, migration, oncogenesis, and angiogenesis.[11] However, the role of PTN in peritoneal fibrosis remains unknown. To elucidate the role of PTN in peritoneal injury, we examined the PTN expression in a mouse model of peritoneal fibrosis and in human peritoneal biopsy samples. We also investigated the functional significance of PTN by using PTN-deficient mice.[13]

RESULTS

To screen novel genes involved in development of peritoneal fibrosis, we compared the gene expression profiles between phosphate buffered saline (PBS)-injected and CG-injected mice three times a week for 3 weeks. As a control, PBS-injected wild-type mice showed no peritoneal fibrosis. CG-injected mice showed marked thickened submesothelial peritoneal membrane compared with PBS-injected mice (Figure 1a, CG-injected mice: 228 μm vs. PBS-injected mice: 34 μm). We performed microarray analysis using parietal peritoneum in mice at 21 days after PBS and CG treatment. We identified genes differentially expressed between PBS- and CG-injected mice, which were also expressed in murine cultured mesothelial cells. Table 1 shows one downregulated and 43 upregulated genes that were expressed by eightfold or greater in CG-treated mice than that in PBS-treated wild-type mice, and which were expressed in the cultured mesothelial

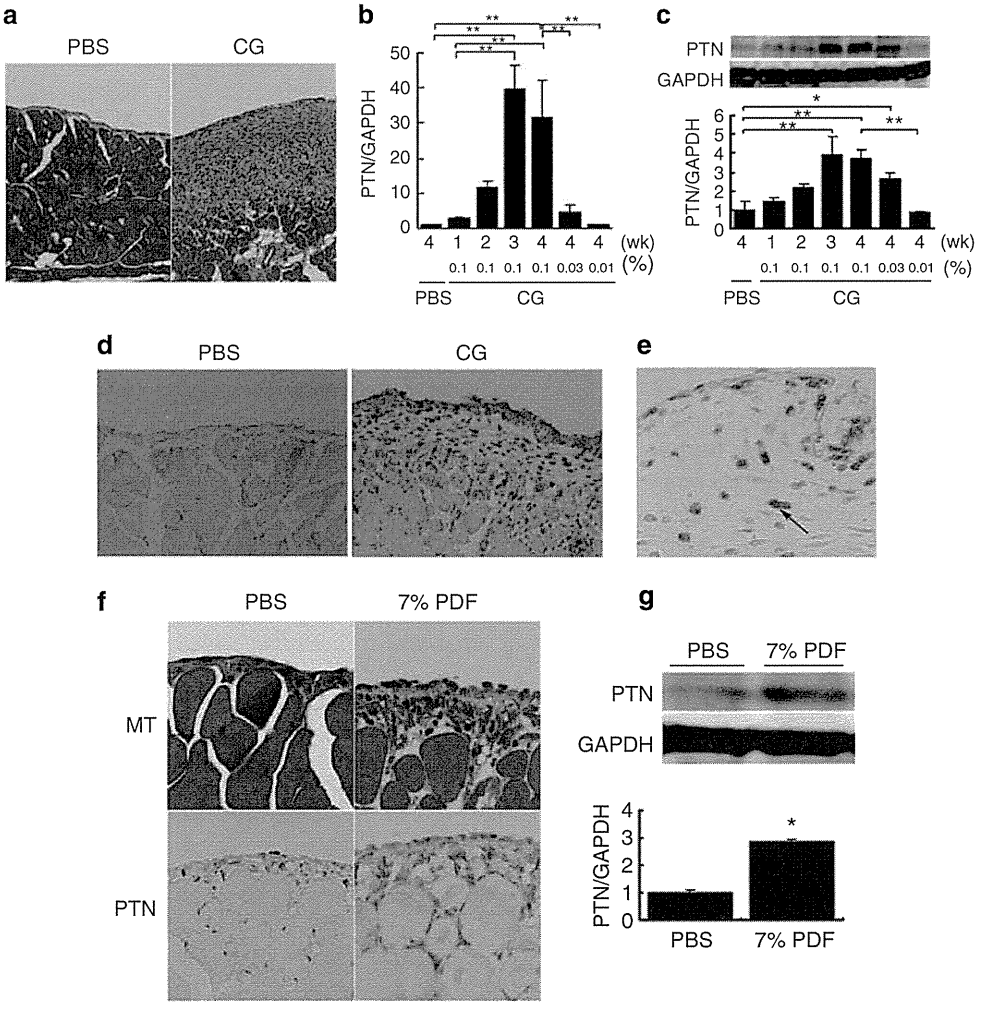

Figure 1 | PTN expression in a mouse model of peritoneal fibrosis. (**a**) Microscopic examination of peritoneal fibrosis model mice. C57BL/6J wild-type mice (WT) treated with phosphate-buffered saline (PBS) showed no fibrosis in the peritoneum. Chlorhexidine gluconate (CG)-treated mice exhibited marked peritoneal fibrosis with moderate infiltration of mononuclear cells on day 21 ($n = 3$, each, original magnification × 20). Pleiotrophin (PTN) mRNA expression (**b**) or protein (**c**) in the peritoneum of PBS- or CG-treated mice was analyzed by real-time reverse transcriptase-polymerase chain reaction analysis or western blot analysis, respectively. GAPDH was used as internal control ($n = 5$, each). (**d**) Immunohistochemical study for PTN (brown). Mesothelial cells and the cells in submesothelial layer were positive for PTN. (**e**) Double immunohistochemical study for PTN (brown) and S100A4 (blue). Some of PTN-positive cells were also positive for S100A4 (arrow). (**f**) Mice receiving daily intraperitoneal injection of 7% peritoneal dialysis fluid (PDF) for 4 weeks showed increased submesothelial layer thickness by Masson's trichrome staining (MT) and upregulated PTN protein in the submesothelial layer ($n = 5$, each). (**g**) Western blot analysis showed that PTN protein in PDF-treated mice was 1.9 times higher than the control. GAPDH was used as internal control. Mean ± s.e. $^*P < 0.05$, $^{**}P < 0.01$ vs. PBS. GAPDH, glyceraldehyde-3-phosphate dehydrogenase; wk, week.

Table 1 | Genes changed in parietal peritoneum in chlorhexidine gluconate (CG)-treated mice compared with phosphate-buffered saline-treated mice after 3 weeks of CG treatment and in the presence of cultured mesothelial cells

Gene title	ID	Fold change of gene up- or downregulated in CG-treated mice compared with PBS-treated mice	Gene symbol
Glucocortoid-regulated inflammatory prostaglandin GH synthase (griPGHS)	M94967	168.897	*Ptgs2*
Procollagen, type VIII, alpha 1	NM_007739	73.51669	*Col8a1*
DEAD (Asp-Glu-Ala-Asp) box polypeptide 3, Y-linked	AA210261	55.71524	*Ddx3y*
Eukaryotic translation initiation factor 2, subunit 3, structural gene Y-linked	NM_012011	48.50293	*Eif2s3y*
A disintegrin and metallopeptidase domain 12 (meltrin alpha)	NM_007400	42.22425	*Adam12*
Interleukin 6	NM_031168	25.99208	*Il6*
Chemokine (C-X-C motif) ligand 1	NM_008176	24.25147	*Cxcl1*
Matrix metallopeptidase 14 (membrane-inserted)	NM_008608	24.25147	*Mmp14*
Chemokine (C-C motif) ligand 7	AF128193	17.14838	*Ccl7*
Ankyrin repeat domain 1 (cardiac muscle)	AK009959	16	*Ankrd1*
Leucine-rich repeat containing 15	AK017350	14.92853	*Lrrc15*
Chemokine (C-C motif) ligand 2	AF065933	14.92853	*Ccl2*
Interferon, alpha-inducible protein	AK019325	14.92853	*G1p2*
Runt-related transcription factor 1	NM_009821	12.12573	*Runx1*
Interferon regulatory factor 7	NM_016850	12.12573	*Irf7*
Collagen triple helix repeat containing 1	AK003674	12.12573	*Cthrc1*
Cytochrome P450, family 7, subfamily b, polypeptide 1	NM_007825	11.31371	*Cyp7b1*
Pleiotrophin	BC002064	11.31371	*Ptn*
Procollagen, type V, alpha 2	AV229424	11.31371	*Col5a2*
Fibronectin 1	BM234360	10.55606	*Fn1*
Chondroitin sulfate proteoglycan 2	NM_019389	10.55606	*Cspg2*
Thrombospondin 1	AI385532	10.55606	*Thbs1*
Membrane-spanning 4-domains, subfamily A, member 4C	NM_022429	10.55606	*Ms4a4c*
Lysyl oxidase	M65143	10.55606	*Lox*
Growth differentiation factor 15	NM_011819	9.849155	*Gdf15*
Dynamin 3, opposite strand	BB542096	9.849155	*Dnm3os*
RNA imprinted and accumulated in nucleus	BB649603	9.849155	*Rian*
WNT1-inducible signaling pathway protein 1	NM_018865	9.849155	*Wisp1*
Secreted frizzled-related sequence protein 1	BI658627	9.849155	*Sfrp1*
Procollagen, type III, alpha 1	AW550625	9.849155	*Col3a1*
Signal transducer and activator of transcription 2	AF088862	9.189587	*Stat2*
2′-5′ Oligoadenylate synthetase-like 2	BQ033138	9.189587	*Oasl2*
Tenascin C	NM_011607	9.189587	*Tnc*
Neural cell adhesion molecule 1	BB698413	8.574188	*Ncam1*
Integrin α5 (fibronectin receptor alpha)	BB493533	8.574188	*Itga5*
Tribbles homolog 3 (*Drosophila*)	BB508622	8.574188	*Trib3*
Gap junction membrane channel protein alpha 1	M63801	8.574188	*Gja1*
Interferon-induced protein with tetratricopeptide repeats 2	NM_008332	8.574188	*Ifit2*
Serine (or cysteine) peptidase inhibitor, clade A, member 3N	NM_009252	8.574188	*Serpina3n*
Lysyl oxidase-like 2	AF117951	8	*Loxl2*
GLI pathogenesis-related 2	BM208214	8	*Glipr2*
2′-5′ Oligoadenylate synthetase-like 1	AB067533	8	*Oasl1*
Tissue inhibitor of metalloproteinase 1	BC008107	8	*Timp1*
Immunoglobulin heavy chain 4 (serum IgG1)	BC008237	0.033493	*Igh4*

cells. Expression of extracellular matrix-related genes, including procollagen type VIII α1, was increased in peritoneal fibrosis model. Inflammatory cytokines including IL-6 were also upregulated. Among these upregulated genes, we focused on secreted proteins. One of them was PTN, which is an 18-kDa secreted protein and has been reported to promote mitogenesis and chemotaxis in cultured cells. Microarray analysis showed that PTN signal in the peritoneal membrane in the CG-injected wild-type mice was upregulated by 11-fold compared with PBS-injected mice (Table 1). Next, we confirmed the increase of PTN mRNA expression in the peritoneum of CG-treated mice by real-time reverse transcriptase-polymerase chain reaction (RT-PCR) analysis (Figure 1b). PTN mRNA in the peritoneum of CG-treated mice was gradually increased and peaked at 3 weeks by 39-fold compared with that in PBS-treated mice at 28 days, and was high until 4 weeks (Figure 1b). Diluted CG, such as 0.03 or 0.01%, induced weaker expression of PTN mRNA than 0.1% CG (Figure 1b). Western blot analysis also showed that PTN protein in the peritoneum of CG-treated mice was gradually upregulated and was highest at 3 weeks by 3.9-fold, as compared with that of PBS-treated mice (Figure 1c). A low concentration of 1:10 diluted CG induced less PTN expression (Figure 1c). Immunohistochemical study showed

that PTN was positive in the spindle-shaped cells and partly in mesothelial cells within the submesothelial layer (Figure 1d). Some of the spindle-shaped cells were also positive for a marker for fibroblasts S100A4, indicating that spindle-shaped cells were fibroblasts (Figure 1e). Next, we examined the effects of infusing peritoneal dialysis fluid (PDF) via a peritoneal catheter on expression of PTN. Mice receiving daily intraperitoneal injection of 7% PDF for 4 weeks showed increased PTN protein in the submesothelial layer with mild peritoneal fibrosis (Figure 1f). PTN protein in PDF-treated mice was 1.9 times higher than control mice, as observed by western blot analysis (Figure 1g).

We examined PTN expression in human biopsy samples at the insertion or removal of peritoneal catheters. PTN was expressed in human peritoneal biopsy samples by RT-PCR method (Figure 2a). Immunohistochemical study showed that PTN was located both in the mesothelial cells (arrows) and in the interstitial cells of peritoneal biopsy samples at the withdrawal from 5-year PD treatment (patient A), which was consistent with a mouse model of peritoneal fibrosis (Figure 2b). We examined whether peritoneal dialysate effluent contained PTN. Western blot analysis showed that peritoneal dialysates from six patients contained 15- and 18-kDa PTN (Figure 2c). The main form of PTN in peritoneal dialysate was 15 kDa. Patient B was a 54-year-old woman suffering from nephrosclerosis with a 2-year PD duration, patient C was a 47-year-old man suffering from diabetic nephropathy with a 2-year PD duration, and patient D was a 29-year-old woman suffering from immunoglobulin A nephropathy with a 1-year PD duration. Next, we examined PD effluent from patients with peritonitis. Patients E and F were 80- and 86-year-old women suffering from peritonitis by *Staphylococcus aureus*, respectively. PD effluents from patients with peritonitis tended to be high PTN levels. These results indicate that PTN exists in human peritoneal membrane and is detectable in peritoneal dialysate effluent.

Next, we investigated functional roles of PTN in cultured mouse peritoneal mesothelial cells. PTN exerts its effect, such as proliferation and chemotaxis, by binding its receptors, RPTPβ/ζ, ALK, and syndecan-3. We examined expression of Ptprz1, which encodes RPTPβ/ζ, ALK, and syndecan-3 in cultured mesothelial cells. Ptprz1 mRNA expression was detected in mesothelial cells but not in fibroblasts, macrophage cell line RAW264.7, mouse T-lymphoma cell line BW5147, mouse B-cell leukemia cell line BCL1-B20, or endothelial cell line bEnd.3 by real-time RT-PCR analyses (Figure 3a). Syndecan-3 mRNA expression was high in mesothelial cells and was also positive in fibroblasts, macrophages, and endothelial cells (Figure 3b). ALK mRNA expression was not detectable. PTN (1 ng/ml) stimulated proliferation in cultured mesothelial cells by 1.7-fold compared with vehicle-treated cells (Figure 3c). Angiotensin II and platelet-derived growth factor-BB stimulation showed less potent activity in cell proliferation than PTN, and endothelial growth factor treatment (100 ng/ml) revealed a similar potency to PTN stimulation (Figure 3c). PTN also induced mesothelial cell migration in the analysis of modified Boyden chamber method by threefold, as compared with vehicle-treated cells (Figure 3d). *In vitro*, fibroblasts cell line NIH3T3 fibroblasts showed higher PTN expression than mesothelial cells. RAW 264.7, mouse BW5147, BCL1-B20, and bEnd.3 showed virtually no expression of PTN (Figure 3e). These results indicate that PTN produced by fibroblasts may exert its biological effect on peritoneal mesothelial cells in the process of peritoneal fibrosis.

Finally, we examined whether PTN has a crucial role in peritoneal fibrosis progression. PTN knockout mice were treated with CG three times a week for 4 weeks. Although the thickness of peritoneal membrane in PTN knockout mice was similar compared with wild-type mice (Figure 4a and b), the expression of tumor necrosis factor-α and IL-1β mRNA was significantly reduced in CG-injected PTN knockout mice at 4 weeks, suggesting that PTN was involved in the inflammatory process (Figure 4c). Furthermore, gene expression of profibrotic factors, TGF-β1, connective tissue growth factor in CG-injected PTN knockout mice was reduced compared with CG-injected wild-type mice (Figure 4c). Fibronectin and type I collagen α1 chain were also decreased in CG-treated

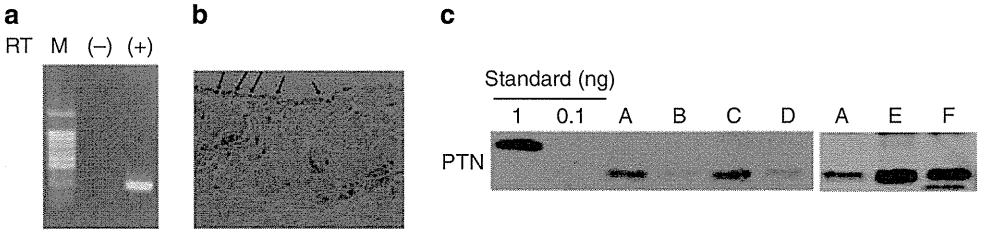

Figure 2 | PTN expression in human peritoneum and in peritoneal dialysate effluent. (**a**) Pleiotrophin (PTN) mRNA expression is detected by reverse transcriptase-polymerase chain reaction in human peritoneal biopsy sample. M, DNA marker (100 bp DNA ladder), RT (–) reverse transcriptase (–), RT (+) reverse transcriptase (+). (**b**) Immunohistochemical study for PTN in the peritoneal biopsy sample from a 5-year peritoneal dialysis (PD) patient A. (**c**) Western blot analysis for PTN in peritoneal dialysate effluent. Patient B was a 54-year-old woman suffering from nephrosclerosis with a 2-year PD duration, patient C was a 47-year-old man suffering from diabetic nephropathy with a 2-year PD duration, and patient D was a 29-year-old woman suffering from immunoglobulin A nephropathy with a 1-year PD duration. Patients E and F suffered from peritonitis by *Staphylococcus aureus*, and their PD efferents were shown on the first day of the peritonitis. Patient E was an 80-year-old woman suffering from nephrosclerosis with a 3-year PD duration. Patient F was an 86-year-old woman suffering from diabetic nephropathy with a 4-year PD duration.

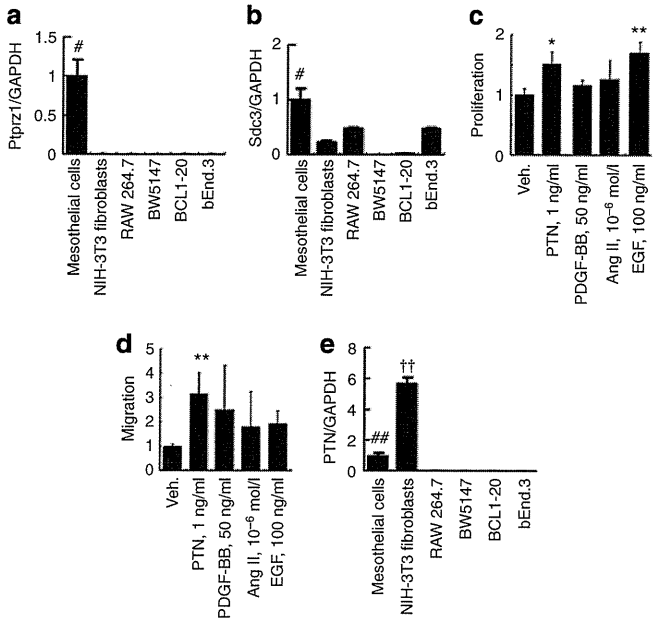

Figure 3 | PTN, Ptprz1, and syndecan-3 expression in cultured cells. The effect of pleiotrophin (PTN) on cell proliferation and migration in cultured mesothelial cells. (**a**) Ptprz1 mRNA expression was quantified by real-time reverse transcriptase-polymerase chain reaction (RT-PCR) in cultured mesothelial cells, NIH3T3 fibroblasts, RAW264.7, BW5147, BCL1-20, and bEnd.3 cells ($n=6$, each). (**b**) Syndecan-3 (Sdc3) mRNA expression was quantified by real-time RT-PCR in cultured mesothelial cells, NIH3T3 fibroblasts, RAW264.7, BW5147, BCL1-20, and bEnd.3 cells ($n=6$, each). (**c**) The effect of PTN on cell proliferation in cultured mesothelial cells. Mesothelial cells were treated with PTN (1 ng/ml), platelet-derived growth factor (PDGF)-BB (50 ng/ml), angiotensin II (Ang II, 10^{-6} mol/l), endothelial growth factor (EGF, 100 ng/ml), or vehicle (Veh.). ^{3}H-thymidine incorporation was assessed ($n=6$, each). (**d**) The effect of PTN on cell migration in cultured mesothelial cells by modified Boyden chamber method. Mesothelial cells were treated with PTN (1 ng/ml), PDGF-BB (50 ng/ml), angiotensin II (10^{-6} mol/l), or EGF (100 ng/ml) ($n=6$, each). (**e**) PTN mRNA expression was quantified by real-time RT-PCR in cultured mesothelial cells, NIH3T3 fibroblasts, RAW264.7, BW5147, BCL1-20, and bEnd.3 cells ($n=6$, each). Mean ± s.e. $^{*}P<0.05$, $^{**}P<0.01$ vs. vehicle. $^{\#}P<0.05$, $^{\#\#}P<0.01$ vs. NIH3T3 fibroblasts, BW264.7, BW5147, BCL1-20 or bEnd.3. $^{\dagger\dagger}P<0.01$ vs. mesothelial cells, RAW264.7, BW5147, BCL1-20 or bEnd.3. GAPDH, glyceraldehyde-3-phosphate dehydrogenase.

PTN knockout mice. On the other hand, expression of type IV collagen α1 chain was increased with the CG injection and was similar between wild-type and PTN knockout mice with CG treatment (Figure 4c). Macrophage infiltration was assessed by immunohistochemical study for F4/80. The number of macrophages in the peritoneum was increased in CG-injected wild-type mice. The number tended to decrease, but not significantly altered in CG-injected PTN knockout mice at 4 weeks (Figure 5a–d and q). In contrast, the number of CD3-positive T cells per the number of total cells in submesothelial area in CG-treated PTN knockout mice was significantly reduced compared with that in CG-treated wild-type mice at 4 weeks (5.6 ± 0.9 vs. 10.3 ± 0.5; Figure 5e–h and r). The effect of PTN on cell proliferation was evaluated by immunohistochemical study for Ki-67, a marker for cell proliferation (Figure 5i–l and s). Interestingly, immunohistochemical study showed that Ki-67-positive cells were localized within submesothelial compact zone and that cells positive for Ki-67 were presumed to be fibroblast-like cells according to their morphological appearance in CG-treated wild-type mice. The number of Ki-67-positive cells in CG-treated PTN-deficient mice was significantly decreased compared with that in CG-treated wild-type mice (1.5 ± 1.1 vs. 3.8 ± 1.2). Collagen IV deposition was similar between CG-treated wild-type mice and CG-treated PTN-deficient mice (Figure 5m–p). Peritoneal equilibration test was conducted to examine the functional role of PTN on peritoneal fibrosis at 2 weeks after the first CG injection. Figure 6 showed that the ratio of creatinine concentrations in the dialysate multiplied by dialysate volume over the plasma creatinine (D Cr × volume/P Cr) in PBS-treated PTN-deficient mice was not different from that in PBS-treated wild-type mice. In contrast, D Cr × volume/P Cr in CG-treated PTN-deficient mice was lower than that in CG-treated wild-type mice (1.93 ± 0.15 vs. 2.33 ± 0.38), suggesting that PTN deficiency was associated with low peritoneal transport in peritoneal fibrosis.

These results suggest that PTN has a crucial role in cell proliferation, extracellular matrix production, and peritoneal permeability during the development of peritoneal fibrosis through inflammatory process.

DISCUSSION

In this study, we identify for the first time that PTN is expressed in peritoneal tissues in mice and humans, especially in experimental peritoneal fibrosis mouse model. Mice receiving intraperitoneal infusion of PDF also showed increased expression of PTN, suggesting that PTN could be involved in peritoneal injury induced by dialysis solution. PTN is an 18- or 15-kDa heparin-binding protein.[11,14] PTN is initially identified as a neurite growth/guidance-regulating protein and belongs to the midkine family.[15,16] PTN has diverse functions including proliferation, mitogenic activities, apoptosis, oncogenic activity, and angiogenic activity.[11] PTN has been shown to have an important role in embryogenesis and kidney development.[17] PTN-deficient mice have been shown to have lower threshold for induction of long-term potentiation in hippocampal slices.[18] Other reports show that PTN-deficient mice exhibit less migration of neutrophils and macrophages to liver after partial hepatectomy,[19] and that female mice deficient in both midkine and PTN are infertile.[13]

The long-term PD can cause deterioration of the peritoneum,[20] and is closely associated with high peritoneal transport rate, which is one of the risk factors for developing encapsulating peritoneal sclerosis.[21] To evaluate the degree of peritoneal damage, several biomarkers have been investigated. Dialysate concentrations of IL-6 and vascular endothelial growth factor have been shown to be associated with increased peritoneal transport rate.[4] Dialysate fibrinogen/